BRAIN
ORIGINAL ARTICLE

Rescue of lysosomal function as therapeutic strategy for SPG15 hereditary spastic paraplegia

Chiara Vantaggiato,[1,†] Genny Orso,[2,†] Giulia Guarato,[2] Francesca Brivio,[1] Barbara Napoli,[2] Elena Panzeri,[1] Simona Masotti,[1] Filippo Maria Santorelli,[3] Maria Lamprou,[4] Sentiljana Gumeni,[4] Emilio Clementi[5] and Maria Teresa Bassi[1]

[†]These authors contributed equally to this work.

SPG15 is a hereditary spastic paraplegia subtype caused by mutations in Spastizin, a protein encoded by the *ZFYVE26* gene. Spastizin is involved in autophagosome maturation and autophagic lysosome reformation and SPG15-related mutations lead to autophagic lysosome reformation defects with lysosome enlargement, free lysosome depletion and autophagosome accumulation. Symptomatic and rehabilitative treatments are the only therapy currently available for patients. Here, we targeted autophagy and lysosomes in SPG15 patient-derived cells by using a library of autophagy-modulating compounds. We identified a rose of compounds affecting intracellular calcium levels, the calcium-calpain pathway or lysosomal functions, which reduced autophagosome accumulation. The six most effective compounds were tested *in vivo* in a new SPG15 loss of function *Drosophila* model that mimicked the reported SPG15 phenotype, with autophagosome accumulation, enlarged lysosomes, reduced free lysosomes, autophagic lysosome reformation defects and locomotor deficit. These compounds, namely verapamil, Bay K8644, 2′,5′-dideoxyadenosine, trehalose, Small-Molecule Enhancer of Rapamycin 28 and trifluoperazine, improved lysosome biogenesis and function *in vivo*, demonstrating that lysosomes are a key pharmacological target to rescue SPG15 phenotype. Among the others, the Small-Molecule Enhancer of Rapamycin 28 was the most effective, rescuing both autophagic lysosome reformation defects and locomotor deficit, and could be considered as a potential therapeutic compound for this hereditary spastic paraplegia subtype.

1 Scientific Institute IRCCS E. Medea, Laboratory of Molecular Biology, 23842 Bosisio Parini, Lecco, Italy
2 Department of Pharmaceutical and Pharmacological Sciences, University of Padova, Largo E. Meneghetti 2, Padova, Italy
3 Department of Molecular Medicine, IRCCS Stella Maris Foundation, Calambrone, 56128 Pisa, Italy
4 Department of Cell Biology and Biophysics, Faculty of Biology, National and Kapodistrian University of Athens, Athens 15784, Greece
5 Unit of Clinical Pharmacology, Department of Biomedical and Clinical Sciences L. Sacco, 'Luigi Sacco' University Hospital, Università di Milano, Milan, Italy

Correspondence to: Chiara Vantaggiato, PhD
Scientific Institute, IRCCS E. Medea, Laboratory of Molecular Biology, Via D. L. Monza 20
23842 Bosisio Parini, Lecco, Italy
E-mail: chiara.vantaggiato@lanostrafamiglia.it

Correspondence may also be addressed to: Genny Orso, PhD
Department of Pharmaceutical and Pharmacological Sciences, University of Padova,

Received March 23, 2022. Revised June 22, 2022. Accepted August 11, 2022. Advance access publication August 27, 2022

Largo E. Meneghetti 2, Padova, Italy
E-mail: genny.orso@unipd.it

Keywords: ALR; SPG15; SMER28; lysosomes; autophagy

Introduction

Hereditary spastic paraparesis (HSPs) are rare neurodegenerative disorders characterized by progressive spasticity and weakness in the lower limbs, due to retrograde axonal degeneration of the corticospinal tracts.[1,2] The high level of genetic heterogeneity with >80 SPG genes being identified corresponds to relatively less mechanistic pathways leading to HSP and including axonal transport, endoplasmic reticulum morphogenesis and function, mitochondrial regulation, myelination, lipid and sterol metabolism, vesicle and endosomal trafficking, lysosomal function and autophagy.[3–7] To date, HSPs remain uncurable conditions and palliative care and rehabilitative programmes are the only available treatments.[8,9]

SPG15 is an autosomal recessive form of HSP with thin corpus callosum and an onset between the first and second decade of life. SPG15 is characterized by slowly progressive spastic paraparesis, mental deterioration associated with cerebellar ataxia, neuropathy and retinal abnormalities, and with distinctive pattern of leukoencephalopathy.[10,11] SPG15 is associated with mutations in the *ZFYVE26* gene that encodes for Spastizin, a large protein that forms a complex with Spatacsin and the adaptor protein 5,[10,12] which mutations are associated, respectively, with SPG11 and SPG48, two clinical subtypes overlapping SPG15.[13–15]

We previously reported autophagy defects in SPG15 patient's derived cells.[16–18] Autophagy is an evolutionarily conserved intracellular process that delivers long-lived proteins and damaged organelles to the lysosomes for degradation through the formation of double-membrane vacuoles termed autophagosomes. After cargo degradation, new lysosomes are generated from autolysosomes by autophagic lysosome reformation (ALR), a process of lysosome biogenesis.[19,20] Tubular structures extrude from the autolysosomes to generate not acidic proto-lysosomes that become functional lysosomes after a maturation process.[19] Constitutive autophagy is essential for neurons and motor neurons to maintain cellular homeostasis and survival,[21,22] such that autophagy and lysosomal defects are associated with several neurodegenerative diseases including Alzheimer's, Parkinson's and Huntington's diseases, spinocerebellar ataxias, amyotrophic lateral sclerosis, different forms of motor neuron diseases and HSP.[23–26]

A role for Spastizin and Spatacsin has been demonstrated in the initial phase of ALR and their loss affects autolysosomal tubulation leading to lysosomal biogenesis defects.[27–29] Loss of Spastizin results in lysosome enlargement, depletion of free lysosomes available to fuse with autophagosomes and autophagosome accumulation in HeLa and SPG15 fibroblast cells.[16,18,27,30,31] Lysosomal abnormalities with reduced tubulation events, lipid accumulation in lysosomal compartment and reduced free lysosomes were reported also in embryonic fibroblasts and cortical neurons of Spastizin knockout mice, associated with defective axonal anterograde transport and impaired neurite outgrowth.[29,31,32]

To date, no pharmacological screening has been performed and no compounds were tested *in vitro* or *in vivo* in SPG15 models. We herein targeted the autophagy-lysosomal pathway in SPG15 cells and in a novel fruit fly model of the disease by using a commercial library of autophagy-modulating compounds. We identified a compendium of drugs, affecting intracellular calcium levels or the calcium-calpain pathway or modulating the lysosomal function, that improved autophagosome degradation in SPG15 cells. When tested *in vivo*, in the fly model of SPG15, the most promising compounds all showed significant improvement of lysosome biogenesis and function. The Small-Molecule Enhancer of Rapamycin 28 (SMER28) did rescue both ALR defects and locomotor deficit *in vivo*.

Materials and methods

Cell cultures and treatments

Fibroblast cell lines were established from skin biopsies obtained from patients carrying L243P, S1312X and R1209fsX SPG15 mutations and from two healthy control individuals as reported.[16] Fibroblasts were grown in Dulbecco's modified Eagle medium (41965062, Invitrogen, Thermo Fisher Scientific) supplemented with 10% FBS (ECS0180DH, Euroclone), 100 U/ml penicillin/streptomycin and 2 mM L-glutamine (15140122 and 25030024, Invitrogen, Thermo Fisher Scientific). Cells were transiently transfected using Lipofectamine 2000 (11668027, Invitrogen, Thermo Fisher Scientific).

Fluorescent cell-based assays

Control and SPG15 cells were seeded in 96-well plates in the concentration of 1500 cells per well and treated for 24 h with compounds from the Screen-Well Autophagy Library (BML-2837, Enzo Life Science) in different concentrations from 1 to 100 μM as indicated, or with dimethyl sulphoxide as a negative control. Autophagy was determined by using the Cyto-ID autophagy detection kit (ENZ-51031, Enzo Life Science) to stain autophagosomes in living cells. Briefly, cells were incubated for 30 min with Cyto-ID Green Detection Reagent and Hoechst 33342 Nuclear Stain in Assay buffer, according to the manufacturer's instructions. Cyto-ID Green and Hoechst fluorescence were quantified by using a Fluoroskan microplate reader (Ascent FL, Thermo Fisher Scientific) at 485/538 and at 355/460 nm, respectively. After background subtraction, Cyto-ID fluorescence was normalized on Hoechst fluorescence. Assay responsiveness was tested in control and SPG15 cells in the presence of 0.2 μM Bafilomycin to block autophagosome degradation or 1 μM Rapamycin to induce autophagy, both for 24 h, or starved in Earle's balanced salt solution for 1 h. We confirmed both the autophagosome accumulation in SPG15 cells and the effect of the autophagy modulators used, indicating the usefulness of the assay for the screening of the library compounds.

Compound toxicity analysis

Compound toxicity was determined by using the CellTiter-Blue Cell Viability Assay (G8080, Promega), according to the manufacturer's instructions. Briefly, cells were seeded in 96-well plates in the concentration of 1500 cells/well. Cells were treated with the selected compounds from the Screen-Well Autophagy Library for 24 h and, the day after, CellTiter-Blue Reagent and Hoechst 33342 were added

directly to the cells and incubated for 1 h a 37°C. The assay is based on the ability of viable cells to reduce the indicator dye resazurin to resorufin, generating a fluorescent product. CellTiter-Blue fluorescence was quantified by using a Fluoroskan microplate reader at 544/590 nm. After background subtraction, CellTiter-Blue fluorescence was normalized on Hoechst fluorescence.

Antibodies and reagents

Anti-LC3B Ab (BK2775) and anti β-actin Ab (sc47778) were purchased from Cell Signaling Technology and Santa Cruz Biotechnology, respectively. Anti-Ref(2)P/p62 Ab (ab17844) was purchased from Abcam. Anti-SQSTM1/p62 Ab (P0067), 2′,5′-dideoxyadenosine (D7408), AICAR (A9978), amiodarone (A8423), Bafilomycin A1 (B1793), (±)Bay K8644 (B112), clonidine hydrochloride (C7897), forskolin (F3917), GF109203X hydrochloride (B6292), minoxidil (M4145), nitrendipine (N144), loperamide hydrochloride (L4762), pimozide (P1793), rolipram (R6520), rilmenidine (R134), SMER28 (S8197), sodium valproate (BP452), spermidine (S2626), suramin sodium salt (S2671), trehalose (T0299), trifluoperazine dihydrochloride (T8516) and verapamil hydrochloride (V4629) were purchased from Merck Life Science.

Confocal immunofluorescence in fibroblast cells

Cells were usually fixed with 4% paraformaldehyde (sc-281692, Santa Cruz Biotechnology) for 10 min and permeabilized with PBS containing 0.1% saponin (S4521, Merck Life Science) and 1% BSA (A9647, Merck Life Science) for 30 min. For the analysis with mRFP-GFP-LC3 vector, cells were fixed with cold methanol for 5 minutes and permeabilized with PBS containing 0.1% Triton X-100 (Merck Life Science). Samples were then incubated for 2 h with primary Abs and revealed using the secondary Abs AlexaFluor-488 and 546 (Invitrogen, Thermo Fisher Scientific). For the staining of LC3-positive vesicles, cells were transfected with the pCMVMAP1LC3B-RFP vector (RC100053, Origene). To analyse autophagosome degradation cells were transfected with the mRFP-GFP-LC3 (ptfLC3) vector, a gift from Tamotsu Yoshimori (Addgene plasmid #21074).[33] For the staining of acidic organelles cells were incubated with 75 nM LysoTracker Red DND-99 (L7528, Invitrogen, Thermo Fisher Scientific) for 5 min to avoid alkalinization (according to the manufacturer's instructions), fixed in paraformaldehyde and processed. Confocal microscopy was performed with a Yokogawa CSU-X1 spinning disc confocal on a Nikon Ti-E inverted microscope equipped with a Nikon ×60/1.40 oil Plan Apochromat objective and were acquired with an Andor Technology iXon3 DU-897-BV EMCCD camera (Nikon Instruments). RFP-LC3 positive vesicles were counted with ImageJ/Fiji by using the 'analyse particles' tool and the investigator was blinded as to the nature of the sample analysed. Lysosomal diameter in fibroblast cells was determined with ImageJ/Fiji by using the straight-line tool to draw a line through lysosomes and then using the plot profile tool. The size of the structures within the profile was determined by using again the straight-line tool. Two regions of interest (ROI)/cell were analysed.

Real-time PCR

Silencing efficiency was analysed in *Drosophila* by quantitative real-time PCR. Total RNA was isolated from 10 larvae with Trizol reagent (Thermo Fisher Scientific) and purified using Direct-Zol TM RNA MiniPrep kit (Zymo Research) according to the manufacturer's instructions. Then, 1 µg/sample was reverse-transcribed into cDNA using the Superscript First Strand Synthesis System for RT–PCR kit (Thermo Fisher Scientific) and random hexamers. The expression levels of *CG5270*, the *Drosophila* orthologue of the human *ZFYVE26* gene, were analysed by quantitative real-time PCR on a QuantStudio™ 3 Real-Time PCR System (Applied Biosystems, Thermo Fisher Scientific) by using a CG5270 specific gene expression assay (Dm02139099_g1, Applied Biosystems, Thermo Fisher Scientific) and RNA polymerase II 140 kD subunit (RpII140, Dm02134593_g1) for normalization. Tubulin-Gal4/+ *Drosophila* line was used as endogenous control. Data were analysed using the delta-delta-Ct method.

SDS-PAGE and western blot

Cells were lysed in Tris-HCl 0.125 M pH 6.8 and 2.5% SDS, loaded on 10 or 15% polyacrylamide gels, blotted onto nitrocellulose membranes and probed with the indicated primary antibodies. Horseradish peroxidase-conjugated secondary antibodies were used and signals were detected using ECL (GE Healthcare).

Fly strains and materials

Fly stocks were raised on standard medium (yeast 27 g/l, agar 10 g/l, corn meal 22 g/l, molasses 66 ml/l, nipagin 2,5 g/l, 12,5 ml/l ethanol 96%) and in standard conditions at 22°C and 12:12 h light:dark cycle. Low caloric nutrient food (yeast 14 g/l, agar 5 g/l, corn meal 11 g/l, molasses 33 ml/l, nipagin 2,5 g/l, 12,5 ml/l ethanol 96%) was prepared to quantify the eclosion rate under starvation. The *Drosophila* strains UAS-GFP-mcherry-Atg8a (BL-37749), UAS-mcherry-Atg8a (BL-37750), Tubulin-Gal4 (BL-5138), W^{1118} (BL-5905) were obtained from the Bloomington Drosophila Stock Center. The UAS-LAMP1-GFP fly line was kindly provided by Helmut Krämer (Department of Neuroscience, University of Texas, Dallas, TX, USA). The UAS-RNAi CG5270 (27390GD) fly line was obtained from Vienna Drosophila Research Center. Gal4/UAS crossings were performed at 28°C.

Drosophila immunohistochemistry and imaging acquisition

Third-instar larvae raised at 28°C were harvested, dissected in HL3, fixed in 4% PFA for 10 min and washed in PBS containing 0.3% Triton X-100 as reported.[34] Larvae were incubated with rabbit anti-Ref2P overnight at 4°C and successively with secondary anti-rabbit Cy^{TM5} Ab (1:500, 111-175-144, Jackson ImmunoResearch Europe Ltd) and DAPI (Invitrogen, Thermo Fisher Scientific) for 1 h at room temperature, washed and mounted on glass slides using Mowiol 4-88 (Merck Life Science). For the staining of acidic organelles third-instar larvae were dissected in HL3, incubated for 15 min in LysoTracker Red DND-99 2 µM (Invitrogen, Thermo Fisher Scientific) and Hoechst 33342 (Sigma-Aldrich), then fixed and mounted. Fixed larvae were acquired using a confocal microscopy ZEISS LSM 800 Confocal Laser Scanning Microscope (Carl Zeiss Microscopy), equipped with a Zeiss 63×/1.4 Plan Apochromat oil objective, by using the ZEN Blue acquisition software.

Lysosome tubulation morphometric analysis

Third-instar feeding larvae expressing the UAS-GFP-LAMP1 or co-expressing the UAS-GFP-LAMP1 and $UAS\text{-}RNA^{sptz}$ using the Tubulin-Gal4 line were individually selected and placed in Petri plates containing a solution of 20% sucrose in PBS for 0, 2, 4, 6 and 8 h. Eight to ten larvae per group were used for ALR quantification. To analyse ALR and quantify autolysosome tubulation we used the

ImageJ/Fiji macro developed to study mitochondrial morphology and to quantify fragmentated/vesicular and elongated mitochondria that derive from fusion and fission processes.[35,36] The green channel of GFP-LAMP1 larvae was extracted to grayscale, thresholded to optimally resolve individual lysosomes and converted to a binary image. The macro traces lysosomal outlines using 'analyse particles' and quantifies size (area), circularity and elongation for each vesicle. Inverse circularity was used as a measure of lysosomal elongation. Elongation describes the shape of a vesicle and a value of one would be considered a perfect circle, while a higher value represents elongated structures. Fragmented mitochondria in the fission controls (cells overexpressing the fission protein Drp1 or depleted of the fusion protein Opa1) have a mean circularity of 0.67, therefore a circularity of 0.7 was used as cut-off to divide circular LAMP1-positive vesicles (≥0.7) from tubulated vesicles (<0.7).[36,37] Elongation was calculated for this latter population that represents tubulated lysosomes. For tubule analysis, the binary image was converted to a skeleton that represents the features in the original image by using the 'skeletonise' tool. Finally, the length of each tubule was determined by using the 'analyse skeleton' plugin and branch length parameter.[38] For each sample, two muscles and two ROI of 2000 μm^2 per muscle were analysed. Eight to ten larvae for each group were used for quantification.

Quantification of autophagosomes, lysosomes and Ref(2)P aggregates in *Drosophila* tissues

Quantification of autophagosomes, lysosomes, acidified lysosomes, free lysosomes and Ref(2)P aggregates was performed as previously described.[39] ImageJ was used to produce a maximum intensity projection of the Z-stack. The UAS-GFP-LAMP1 strain was used to quantify the number and size of lysosomes, whereas the UAS-mcherry-Atg8a strain was used to quantify the number of autophagosomes. For lysosomes, autophagosomes and Ref(2)P aggregates quantification, ImageJ was used to threshold the red, green and cyano channels and to count GFP, mcherry and Cy5 dots. For each sample, two muscles and two ROI of 2000 μm^2 per muscle were analysed. For each brain, three ROI of 3400 μm^2 were analysed. Eight to ten larvae for each group were used for quantification. The colocalization of lysosomes with autophagosomes was calculated using the colocalization function of ImageJ (coloc-2). Colocalizing dots obtained from the macro were quantified and normalized on the total number of autophagosomes (red dots).

Drosophila drug treatments

To identify the most effective and not toxic concentration for each compound we carried out two experiments: the first pilot test was done to distinguish between the toxic and non-toxic range of concentration, in the subsequent experiment we identified the concentration that allowed a correct development of *Drosophila* into the adult stage. Supplementary Table 5 summarizes the concentrations tested and the relative effects on development, lethality and eclosion rate. Verapamil and Bay K8644 previously dissolved in ethanol were added to standard *Drosophila* food at the final concentration of 1 and 0.4 μM, respectively. 2′,5′-Dideoxyadenosine and SMER28 were dissolved in dimethyl sulphoxide and added to standard food at the final concentrations of 30 and 20 μM. Trehalose and

Table 1 Effect of the 23 selected compounds on autophagosome fluorescence and cell vitality in SPG15 cells

Compounds	Cyto-ID fluorescence	Cell titer-blue fluorescence
Control cells	$0.407376 \pm 0.01946^{***}$	1.009622 ± 0.02678
SPG15 untreated cells	$1 \pm 0.03269^{+++}$	1 ± 0.02729
(±)Bay K8644 10 μM	$0.750333 \pm 0.08544^{**,+++}$	1.098417 ± 0.17490
2′,5′-Dideoxyadenosine 10 μM	$0.605417 \pm 0.02858^{***}$	1.029107 ± 0.04596
AICAR 10 μM	$0.682257 \pm 0.03742^{***,+}$	1.235116 ± 0.17384
Clonidine·HCl 10 μM	$0.741703 \pm 0.03266^{***,+++}$	1.026005 ± 0.01879
Fluspirilene 10 μM	$0.781212 \pm 0.01633^{*,+++}$	0.994232 ± 0.09926
Forskolin 10 μM	$0.660783 \pm 0.00712^{***}$	1.128379 ± 0.19912
Lithium chloride 10 μM	$0.783827 \pm 0.03629^{*,+++}$	1.042487 ± 0.06664
Loperamide·HCl 10 μM	$0.769407 \pm 0.08287^{**,+++}$	1.012879 ± 0.03077
Minoxidil 10 μM	$0.710553 \pm 0.02449^{***,++}$	1.058033 ± 0.01659
Nitrendipine 10 μM	$0.791688 \pm 0.05715^{*,+++}$	1.101974 ± 0.01774
Pimozide 20 μM	$0.832484 \pm 0.02055^{*,+++}$	0.842045 ± 0.13175
Quinine HCl·2H_2O 10 μM	$0.771528 \pm 0.01414^{**,+++}$	1.118622 ± 0.04515
Rilmenidine 10 μM	$0.763333 \pm 0.02867^{**,+++}$	0.995853 ± 0.02012
Rolipram 10 μM	$0.781676 \pm 0.06096^{*,+++}$	1.113576 ± 0.01586
SB216763 20 μM	$0.762309 \pm 0.02677^{**,+++}$	0.980215 ± 0.01855
SMER28 10 μM	$0.630783 \pm 0.05354^{***}$	0.885013 ± 0.00783
Sodium valproate 10 μM	$0.650599 \pm 0.00816^{***}$	0.967541 ± 0.02448
Spermidine 10 μM	$0.765055 \pm 0.02944^{**,+++}$	0.908491 ± 0.12057
Suramin·6Na 10 μM	$0.721689 \pm 0.04143^{***,++}$	1.16602 ± 0.05748
Tolazamide 10 μM	$0.751173 \pm 0.07789^{**,+++}$	1.199667 ± 0.05472
Trehalose 10 μM	$0.582542 \pm 0.03559^{***}$	0.936267 ± 0.01455
Trifluoperazine·2HCl 10 μM	$0.692157 \pm 0.00816^{***,+}$	0.929301 ± 0.13947
Verapamil·HCl 10 μM	$0.710291 \pm 0.09416^{***,++}$	0.954414 ± 0.02196
Staurosporine 1 μM	–	0.750517 ± 0.01454

The autophagosome fluorescence and cell vitality of SPG15 cells treated with the 23 selected compounds are reported. SPG15 cells were incubated with the compounds for 24 h at the indicated concentrations and successively with the Cyto-ID Green reagent, to stain autophagosomes or with the CellTiter-Blue reagent, for cell vitality. Cyto-ID and CellTiter-Blue fluorescence levels were normalized on Hoechst fluorescence and are reported as fold increases of SPG15 untreated cells (=1). No differences were detected among L243P, S1312X and R1209fsX SPG15 mutated cells and the results shown are the mean. For cell vitality assay the apoptosis inducer staurosporine was used as a negative control. The statistical analysis is reported (one-way ANOVA followed by Dunnett's multiple comparison test; $n > 3$ experiments; *versus SPG15 untreated cells; +versus control cells).

trifluoperazine dihydrochloride were dissolved in ddH_2O and added to standard food at the final concentration of 200, or 500 and 300 μM.

Eclosion rate

Female virgins and males were placed in a vial in a 10:5 ratio and allowed to lay eggs for 48 h. Then, adults were discarded and larvae allowed to develop. Pupae were counted and flies that successfully eclosed were scored, and data expressed as percent of eclosion (number of adult flies eclosed/number of pupae). Six vials for each genotype were used.[40]

Negative geotaxis assay

For climbing assays, 20 flies for each genotype were collected after hatching and were transferred every other day to vials containing fresh standard or drug enriched food. Climbing capability was tested at three times along life of these flies (5, 10 and 15 days of age). *Drosophilae* were placed in an empty plastic vial with a line drawn 8 cm from the bottom of the tube and allowed to recover from anaesthesia for 1 h. Flies were gently tapped to the bottom of the tube and the number of flies above the 8 cm mark at 7 s was recorded as a percentage of flies able to climb the vial. Ten separate and consecutive trials were performed, and the results were averaged. At least 100 flies were tested for each genotype.[41]

Lifespan assay

We collected newly eclosed animals and bred them at low density (<20 animals per vial) in standard conditions. Ageing animals were transferred to new vials three times per week, with deaths scored. Lifespan plots were generated by calculating the percentage of survivorship and plotting viability as a function of time.[41]

Statistics

Double-blind experiments were performed. We report no data exclusion. Student's *t*-test for unpaired variables (two-tailed) and one-way ANOVA or two-way ANOVA followed by Dunnett's, Tukey's or Sidak's multiple comparisons tests were performed using GraphPad Prism v.9.3.0 for Windows (GraphPad Software, San Diego, CA, USA). Results are reported as individual data plus the mean ± SEM; *n* represents individual data, as indicated in each figure legend. *P*-values of <0.05 were considered significant. Individual *P*-values are indicated in the graphs ($^{+}$, $^{*}P < 0.05$; $^{++}$, $^{**}P < 0.01$; $^{+++}$, $^{***}P < 0.001$). Statistics are reported in each figure legend.

Study approval

The human tissues were harvested following written informed consent from all participants. All experimental procedures were approved by the IRCCS E. Medea Scientific Institute Ethics Committee.

Data availability

Data supporting the findings of this study are included in this paper and Supplementary material. All supporting data are available from the corresponding authors on reasonable request.

Results

Screening of the autophagy library compounds and validation in SPG15 cells

Autophagosome maturation in SPG15 cells is impaired due to autophagy and ALR defects that reduce the number of lysosomes available for degradation and induce autophagosome accumulation.[16–18,27] We performed a pilot screening of a small library of 94 compounds with a defined autophagy inducing or inhibitory activity (Supplementary Table 1) for their ability to reduce autophagosome accumulation in SPG15 cells. We identified 23 non-toxic compounds that induced a significant reduction in autophagosome fluorescence in patient-derived SPG15 cells carrying the point mutation L243P or one of the two truncating mutations S1312X and R1209fsX, previously characterized (Table 1 for the selected 23 compounds; Supplementary Tables 2 and 3 for all the compounds of the library).[16–18] We classified these compounds into three different groups on the basis of their mechanism of action, i.e. compounds that: (i) affect intracellular calcium levels; (ii) affect the calcium-calpain-$G_{S\alpha}$ and cyclic AMP (cAMP)-Phospholipase C ϵ isoform (PLCϵ)-inositol 1,4,5-triphosphate (IP3) pathways; and (iii) promote autophagosome degradation; thereby highlighting the importance of these pathways in the regulation of autophagy in SPG15 cells.[23,42–45] The effects of the 23 compounds identified were analysed more in detail in SPG15 cells by quantifying the autophagosomal markers LC3-II and SQSTM1/p62, and determining the autophagosome number by immunofluorescence.

Compounds affecting intracellular calcium levels

This group includes verapamil, loperamide, nitrendipine, fluspirilene and pimozide that reduce intracellular calcium levels and induce mTOR-independent autophagy,[42,46–49] and Bay K8644, minoxidil, tolazamide and quinine that inhibit calcium channels and autophagy.[42,49] Their mechanisms of action are schematized in Fig. 1A.

All compounds belonging to this group reduced LC3-II levels and autophagosome accumulation in SPG15 cells (Fig. 1B–D). Among the others, verapamil, loperamide, Bay K8644 and tolazamide were the most effective compounds in reducing LC3-II, p62 levels and the number of autophagosomes to values similar to control cells (Fig. 1B–E). Nitrendipine, fluspirilene, minoxidil and tolazamide did not reduce p62 levels (Fig. 1C) and increased the percentage of p62 vesicles that do not colocalize with autophagosomes, compared with SPG15 untreated cells (Fig. 1F). These vesicles may represent isolation membranes and/or p62-ubiquitinated-protein aggregates directed to ubiquitin-proteasome system degradation.[50,51]

Compounds affecting the calcium-calpain-$G_{S\alpha}$ and cAMP-PLCϵ-IP3 pathways

The compounds of the second group affect autophagy by regulating cAMP levels, inositol 1,4,5-triphosphate (IP3) levels or AMP-dependent Kinase (AMPK) activity,[48,52,53] as depicted in Fig. 2A. 2′,5′-dideoxyadenosine (2′5′ ddA), suramin, clonidine and rilmenidine reduce cAMP levels inducing autophagy, while rolipram and forskolin increase them.[42,52] Sodium valproate and lithium chloride reduce inositol and IP3 levels, enhancing the clearance of autophagy substrate.[53,54] Finally, spermidine and AICAR both activate AMPK, but have an opposite effect on autophagy, due to their different effect on Beclin1.[55–57]

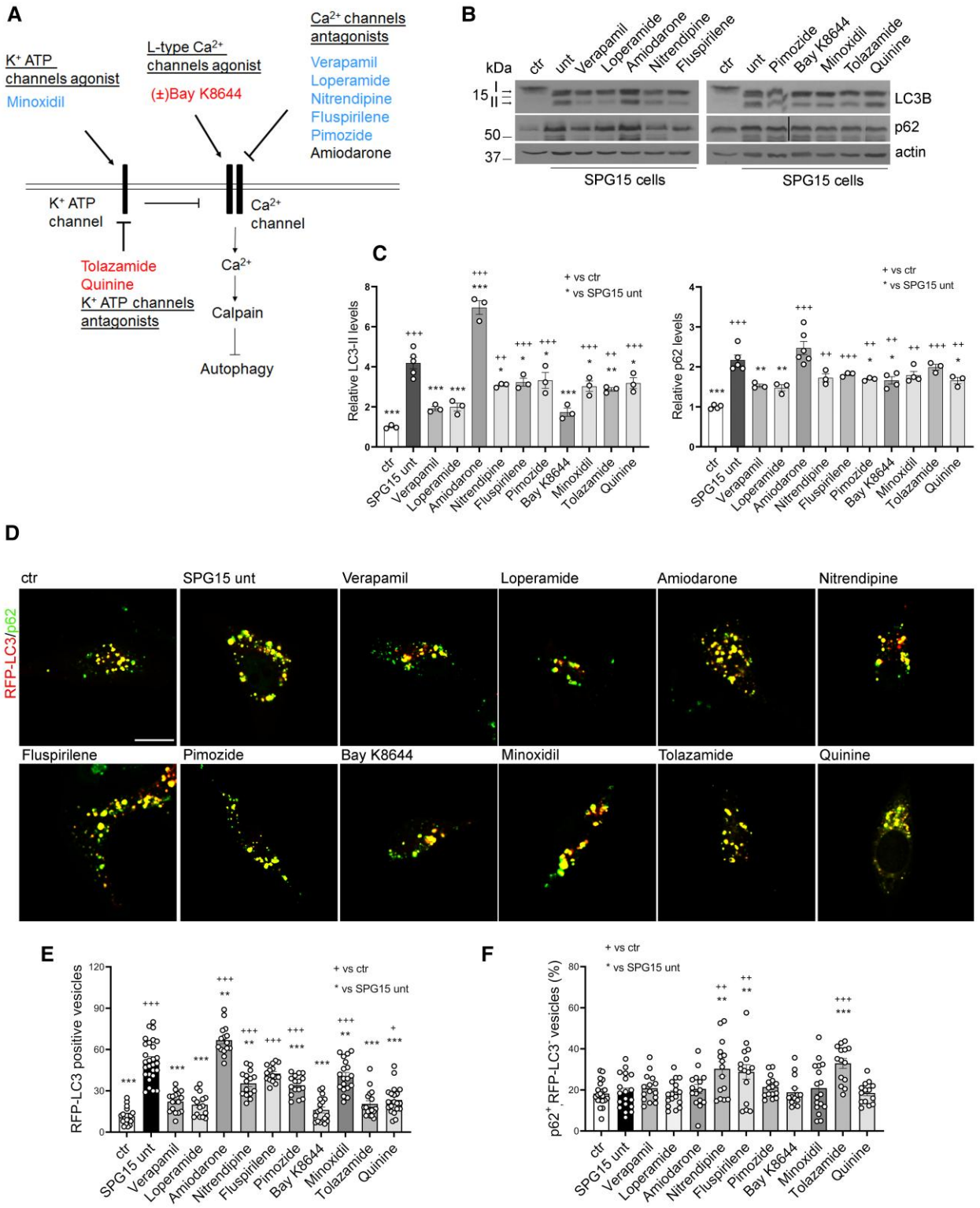

Figure 1 Compounds that affect intracellular calcium channels. (**A**) Schematic representation of the mechanism of action of the compounds of this group. Red and blue indicate the compounds that inhibit or activate autophagy, respectively. (**B**) SPG15 cells were incubated with the indicated compounds at the concentration of 10 μM for 24 h (except of pimozide, 20 μM). Amiodarone, an L-type calcium channel antagonist that we found to increase autophagosome fluorescence in high-throughput screening (Supplementary Table 2), was used as a negative control. (**C**) Total protein extracts were immunoblotted as shown, and LC3-II and SQSTM1/p62 levels were normalized on actin levels and expressed as fold increase of control cells (one-way ANOVA followed by Dunnett's multiple comparison test; $n = 3$ experiments; *versus SPG15 unt; +versus ctr). Black line indicates lanes that were run on the same gel but were non-contiguous. Uncropped gels are in Supplementary Fig. 1. (**D**) SPG15 cells were transfected with the pCMVMAP1LC3B-RFP vector for the staining of autophagosomes (red), incubated with the indicated compounds for 24 h, fixed and stained with anti-SQSTM1/p62 (green) Ab. Yellow in the images indicates colocalization. Scale bar = 10 μm. (**E**) RFP-LC3 positive vesicles are reported in the graph (one-way ANOVA followed by Dunnett's multiple comparison test, $n > 15$ cells; *versus SPG15 unt; +versus ctr). (**F**) p62 vesicles not colocalizing with LC3 were counted, normalized on total number of p62 vesicles and reported as percentage (one-way ANOVA followed by Dunnett's multiple comparison test, $n > 15$ cells; *versus SPG15 unt; +versus ctr).

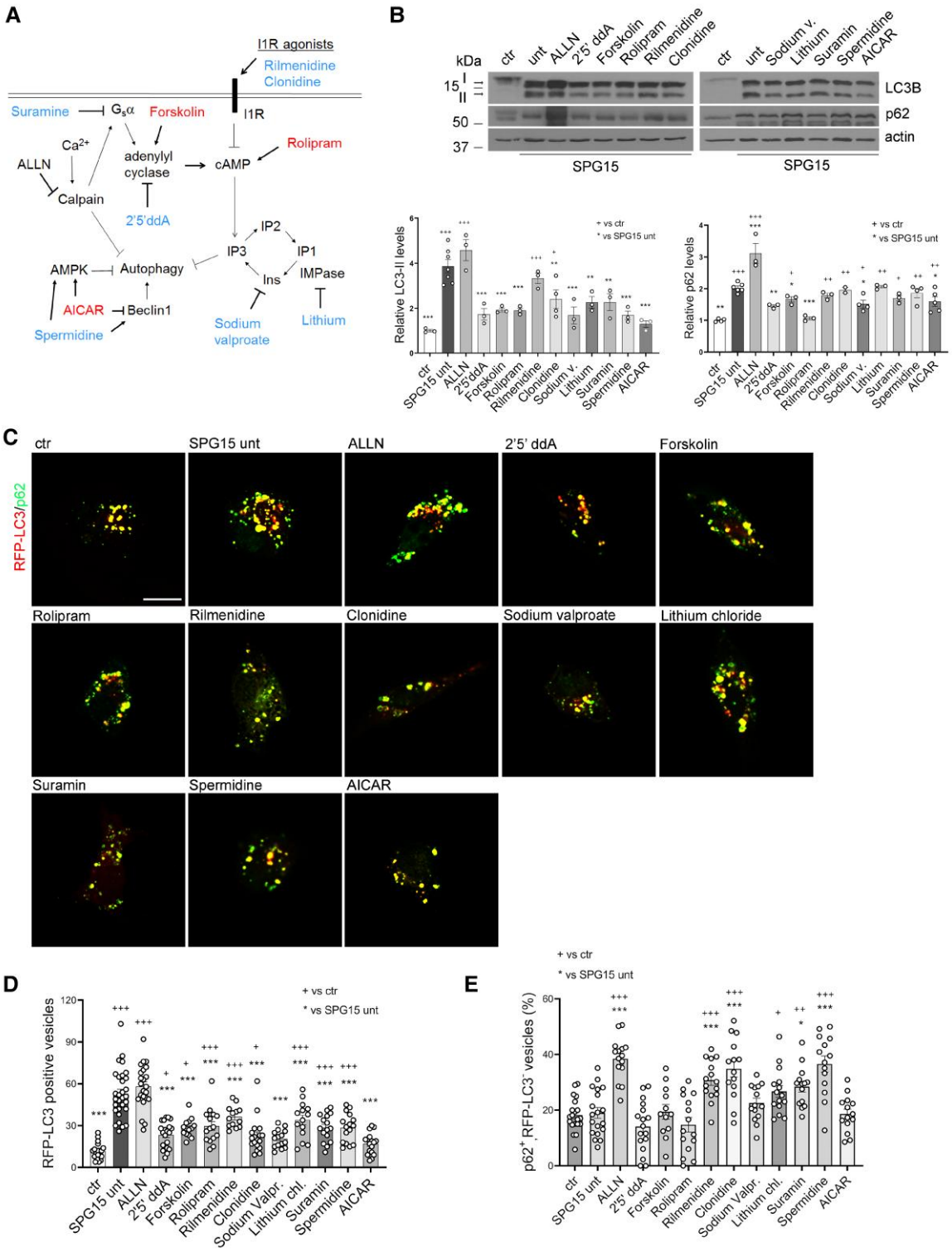

Figure 2 Compounds affecting calcium-calpain-$G_{s\alpha}$ and cAMP-PLCε-IP3 pathways. (**A**) Schematic representation of the mechanism of action of the compounds of this group. Red and blue indicate the compounds that inhibit or activate autophagy, respectively. (**B**) SPG15 cells were incubated with the indicated compounds at the concentration of 10 μM for 24 h and total protein extracts were immunoblotted as shown. ALLN, a calpain inhibitor that increased autophagosome fluorescence in the high-throughput screening (Supplementary Table 2), was used as a negative control. LC3-II and SQSTM1/p62 levels were normalized on actin levels and expressed as fold increase of control cells (one-way ANOVA followed by Dunnett's multiple comparison test; $n = 3$ experiments; *versus SPG15 unt; +versus ctr). Uncropped gels are in Supplementary Fig. 2. (**C**) SPG15 cells were transfected with the pCMVMAP1LC3B-RFP vector to stain autophagosomes (red), incubated with the indicated compounds for 24 h, fixed and stained with anti-SQSTM1/p62 (green) Ab. Yellow in the images indicates colocalization. Scale bar = 10 μm. (**D**) RFP-LC3 positive vesicles quantification from **C** is reported in the graph (one-way ANOVA followed by Dunnett's multiple comparison test; $n > 15$ cells; *versus SPG15 unt; +versus ctr). (**E**) p62 vesicles not colocalizing with LC3 were counted, normalized on total number of p62 vesicles and reported as percentage (one-way ANOVA followed by Dunnett's multiple comparison test, $n > 15$ cells; *versus SPG15 unt; +versus ctr).

We found that LC3-II levels and the number of autophagosome accumulated in SPG15 cells were reduced by all the compounds, independently of their targets, with 2′,5′-dideoxyadenosine, forskolin, sodium valproate and AICAR as the most efficient, also in inducing cargo degradation (Fig. 2B–D). Similar to other compounds of the first groups, rilmenidine, clonidine, lithium chloride, suramine and spermidine did not induce a significant reduction of p62 levels (Fig. 2B) and increased the percentage of p62 vesicles negative for RFP-LC3, compared with SPG15 untreated cells (Fig. 2E).

Compounds that promote autophagosome-lysosome fusion

The third group includes compounds promoting autophagosome-lysosome fusion and degradation (Fig. 3A). Trehalose and trifluoperazine induce Transcription Factor EB (TFEB) nuclear translocation,[58,59] a transcription factor that activates lysosomal and autophagy genes inducing lysosome biogenesis and promoting autophagosome-lysosome fusion.[60] SB216763 induces autophagy and promotes autophagic clearance by inhibiting Glycogen Synthase Kinase 3 beta (GSK3β),[61] a TFEB negative regulator.[62,63] The small-molecule enhancer of autophagy SMER28 induces autophagosome synthesis and clearance.[64,65]

We found that all the compounds decreased LC3-II levels and the number of accumulated autophagosomes in SPG15 cells at similar threshold levels (Fig. 3B–D), but SB216763 did not reduce p62 levels; it increased the percentage of p62 vesicles negative for RFP-LC3 (Fig. 3E).

Effect of the hit compounds on autophagosome degradation and lysosome enlargement

Spastizin mutations affect ALR and SPG15 cells show lysosome enlargement, a decreased number of free lysosomes and autophagosome accumulation.[16,27,31,32] Therefore, we analysed the effects of the 23 selected compounds on autophagosome degradation by using the mRFP-GFP tandem fluorescent tagged LC3B vector to visualize autophagosomes.[18] The GFP signal is sensitive to acidic compartment and is quenched when autophagosomes fuse with lysosomes, thus forming autolysosomes.[18] We found that a very low percentage of the autophagosome accumulated in SPG15 cells are red acidified functional autolysosomes (mRFP$^+$, GFP$^-$) compared to control cells, and that verapamil, Bay K8644, 2′,5′-dideoxyadenosine, sodium valproate, lithium chloride, trehalose, SMER28, SB216763 and trifluoperazine significantly increased the percentage of red acidified autolysosomes with respect to SPG15 untreated cells (Fig. 4A and B). These compounds induced a decrease in total mRFP-LC3 vesicles number in SPG15 cells (Supplementary Fig. 4B and Fig. 1E, 2D and 3D) by improving lysosomal function and promoting autophagosome degradation; indeed, they reduced the number of autophagosomes (mRFP$^+$, GFP$^+$) (Supplementary Fig. 4C) and increased the absolute number of autolysosomes (mRFP$^+$, GFP$^-$) (Supplementary Fig. 4D) compared with SPG15 untreated cells.

SPG15 cells presented enlarged LAMP1 positive vesicles, compared with control,[27,32] that principally represent lysosomes,[31] as confirmed by the use of the acidic organelle marker LysoTracker (Supplementary Fig. 5). This staining evidenced also the presence of a small population (20%) of enlarged LAMP1 vesicles that are not acidic and could therefore represent late endosomes or amphisomes fused with this latter population.[66] We analysed the effect of the selected compounds on the size of the LAMP1 positive vesicles and we found that verapamil, Bay K8644, 2′,5′-dideoxyadenosine, trehalose, SMER28 and trifluoperazine significantly reduced the lysosomal diameter in SPG15 cells to values similar to the control (Fig. 4C). Therefore, these compounds were selected for the *in vivo* analysis.

The SPG15 *Drosophila* model shows locomotor deficit, autophagosome accumulation and ALR defects

To investigate the *in vivo* efficacy of the selected compounds, we developed and characterized a novel SPG15 *Drosophila* model. *CG5270* is the predicted *Drosophila* orthologue of the human *ZFYVE26*. Its functional domain displays a 51% identity with the FYVE domain of the human protein (Supplementary Fig. 6 and Supplementary Table 4) and is predicted to enable phosphatidylinositol-3-phosphate binding activity.[67]

We adopted a loss of function approach by ubiquitously expressing an RNAi construct that strongly reduced (70%) the expression of *CG5270* (Supplementary Fig. 7). We analysed the eclosion rate of the RNAi^{CG5270} line and we found that while in standard condition the eclosion rate of RNAi^{CG5270} line was similar to control flies, it was significantly reduced under nutrient restriction, suggesting that these flies are sensitive to starvation (Fig. 5A). Moreover, we found that the activity index measured by the negative geotaxis assay, was drastically decreased in RNAi^{CG5270} flies (Fig. 5B), a phenotype often presents in *Drosophila* models of HSP and neurodegenerative disorders.[68–70,39]

We then coexpressed the mcherry-GFP-Atg8a and the RNAi^{CG5270} using the tubulin-Gal4 driver line to analyse autophagosome accumulation and fusion in larval muscle, a well-studied *Drosophila* tissue for the analysis of autophagy and lysosomal function.[71,72] Our data indicate that the reduction of *CG5270* expression levels induced a significant increase in total Atg8 vesicles number and in the percentage of autophagosomes (yellow, mcherry$^+$, GFP$^+$ Atg8 vesicles), and a decrease in the percentage of autolysosomes (red, mcherry$^+$, GFP$^-$ Atg8 vesicles) (Fig. 5C and D), indicating defects in autophagosome degradation. We then quantified lysosomal/late endosomal alterations by expressing the recombinant line GFP-LAMP1; mcherry-Atg8a (Fig. 5E and F). RNAi^{CG5270} larvae muscles presented an increase in LAMP1 positive vesicles size and number compared with control (Fig. 5F), a reduced percentage of free LAMP1 positive vesicles and an increase in Atg8a/LAMP1 colocalizing vesicles, most likely autophagosomes fused with late endosomes, consistent with the reduced percentage of autolysosomes observed in the RNAi^{CG5270} larvae muscles (Fig. 5D). Indeed, the use of LysoTracker to stain acidic organelles in the GFP-LAMP1 line showed that ∼50% of the LAMP1 vesicles both in control and RNAi^{CG5270} larvae muscles were not labelled by LysoTracker (Supplementary Fig. 8), consistent with previous data.[72] Therefore, these vesicles are not lysosomes or autolysosomes, but could represent endo-lysosomal structures, immature autophagosomes fused with late endosomes or new formed lysosomes.[19,66]

We also analysed ALR *in vivo* by visualizing and measuring lysosomes and the tubular structures that extrude from the autolysosomes to generate proto-lysosomes during starvation,[19] taking advantage of an ImageJ/Fiji macro previously described to quantify mitochondrial fission and fusion events.[35–37] In our analysis, time course experiments were performed on muscle of third-instar feeding larvae expressing GFP-LAMP1 that were starved for 2, 4, 6 and 8 h (Fig. 5G).[19,20] Area and circularity of LAMP1 positive vesicles and the elongation index of tubulated vesicles were quantified and are reported in Supplementary Fig. 9. In the control line we clearly identified two vesicle populations: round and small vesicles with stable value of area and circularity (presumably not involved in ALR), and a population of vesicles that increased in size and

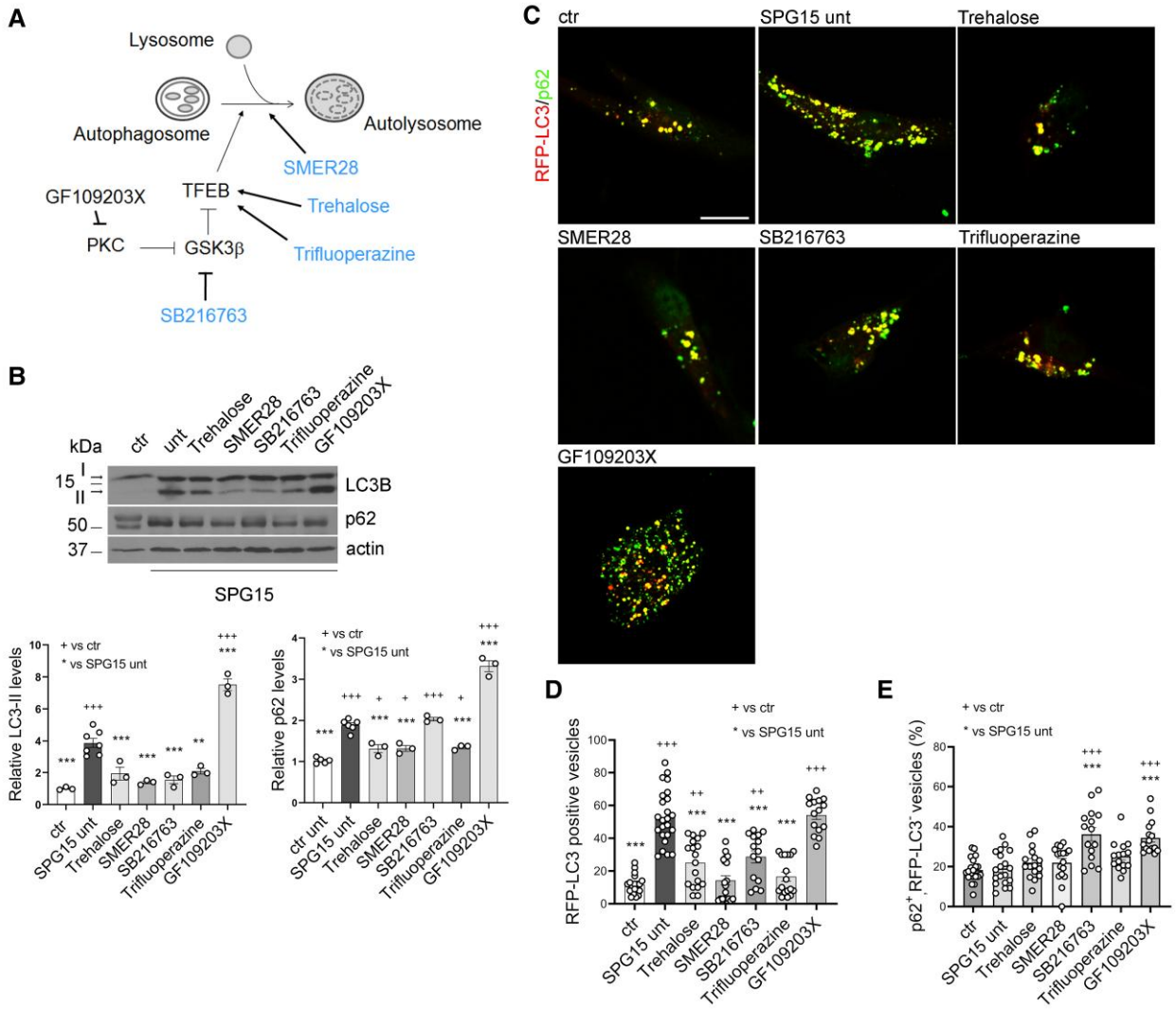

Figure 3 Compounds affecting autophagosome degradation. (**A**) Schematic representation of the mechanism of action of the compounds of this group. (**B**) SPG15 cells were incubated with the indicated compounds at the concentration of 10 μM, except of SB216768 (20 μM), for 24 h and total protein extracts were run on SDS–polyacrylamide gels and probed with anti-MAP1LC3B, SQSTM1/p62 and actin Abs. GF109203X, a PKC inhibitor that increased autophagosome fluorescence in the high-throughput screening (Supplementary Table 2), was used as a negative control. LC3-II and SQSTM1/p62 levels were normalized on actin and expressed as fold increase of control cells (one-way ANOVA followed by Dunnett's multiple comparison test, $n = 3$ experiments; *versus SPG15 unt; +versus ctr). Uncropped gels are in Supplementary Fig. 3. (**C**) SPG15 cells were transfected with the pCMVMAP1LC3B-RFP vector for the staining of autophagosomes, incubated with the indicated compounds for 24 h, fixed and stained with anti-SQSTM1/p62 (green) Ab. Yellow in the images indicates colocalization. Scale bar = 10 μm. (**D**) RFP-LC3 positive vesicles are reported in the graph (one-way ANOVA followed by Dunnett's multiple comparison test; $n > 15$ cells; *versus SPG15 unt; +versus ctr). (**E**) p62 vesicles not colocalizing with LC3 were counted, normalized on total number of p62 vesicles and reported as percentage (one-way ANOVA followed by Dunnett's multiple comparison test, $n > 15$ cells; *versus SPG15 unt; +versus ctr).

decreased in circularity along with time as the starvation proceeded (suggested to be tubulated vesicles) (Supplementary Fig. 9A). In control larvae we found that after a short term of starvation (2 and 4 h) lysosomes increased in size (Supplementary Fig. 9A), consistent with the inhibition of mTOR, as reported for other *in vitro* and *in vivo* models,[19] and presented tubule extrusion after 6 h of nutrient deprivation (Fig. 5G and Supplementary Fig. 9B), consistent with autophagy reactivation allowing lysosomal reformation.[73] Finally, after 8 h we detected only small LAMP1 positive vesicles, more likely new formed lysosomes (Fig. 5G). Conversely, the RNAi^{CG5270} line, other than a population of round and small vesicles similar to that of control line, presented a population of enlarged vesicles stable in size and circularity along with time (Supplementary Fig. 9A). Moreover, at 6 h of starvation there was no vesicle tubulation (Fig. 5G–J), indicating a block of lysosomal reformation in line with the altered ALR process previously described in SPG15 models.[27,29,31,32] Indeed, the elongation indexes of tubulated vesicle (Fig. 5H) and tubule length (Fig. 5I) were reduced in RNAi^{CG5270} larvae; likewise, the percentage of vesicles with tubules >1 μm (Fig. 5J) decreased compared with control. This clearly highlights that a reduced *CG5270* expression is associated with the inability to form new tubulated structures from preexisting lysosomes.

A defective autophagic cargo clearance was also confirmed in the brain; indeed, we found accumulation of Ref(2)P/p62-positive aggregates in RNAi^{CG5270} larval ventral nerve cord (Fig. 5K and L).

In conclusion, downregulation of *CG5270* expression levels mimicked the SPG15 phenotype with autophagy and locomotor

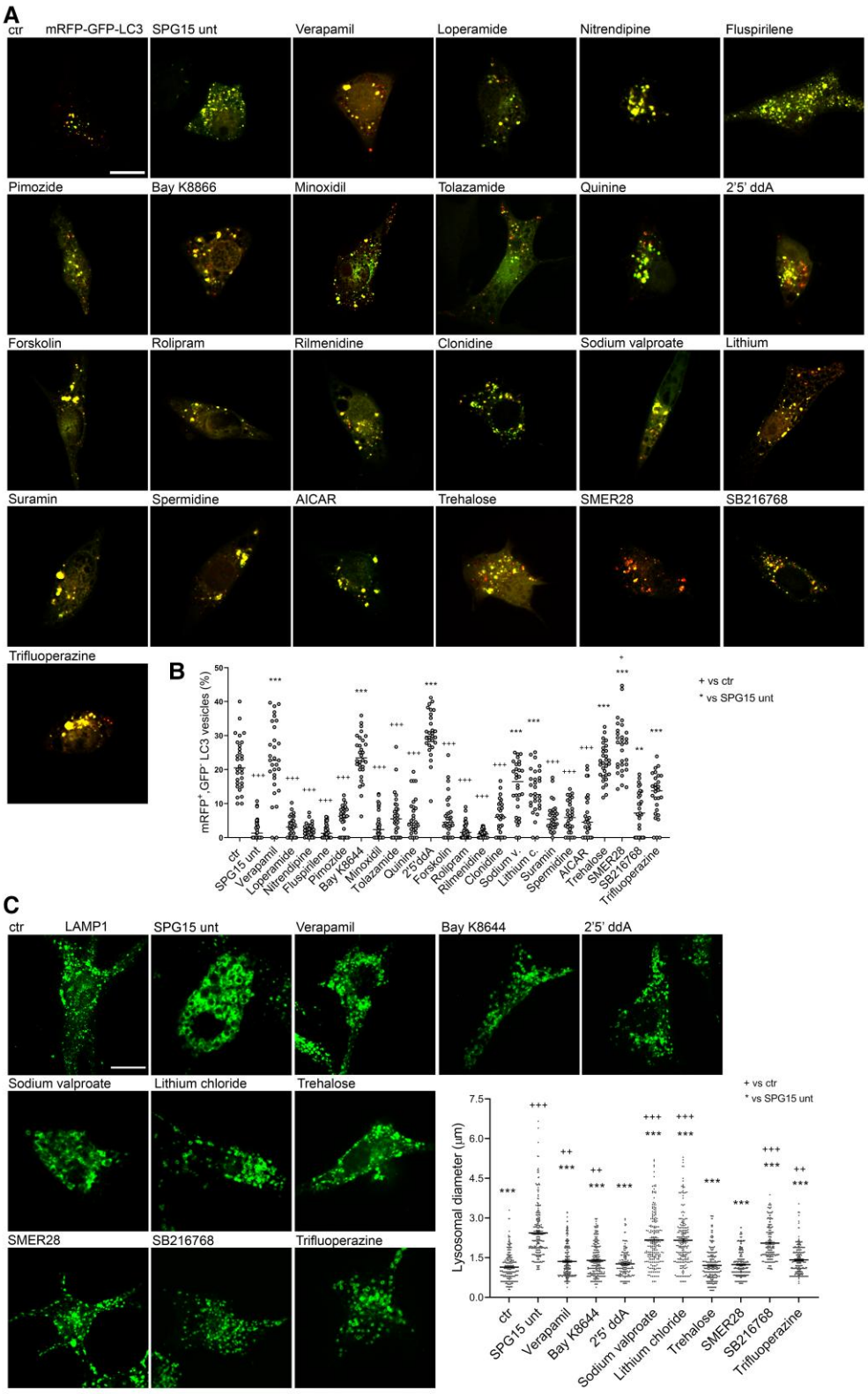

Figure 4 Effect of the selected compounds on autophagosome degradation and lysosomal size. (**A**) SPG15 mutated cells were transfected with the mRFP-GFP-LC3 vector and incubated with the indicated compounds for 24 h. Cells were then fixed and analysed by confocal microscopy. mRFP-GFP-LC3 positive autophagosomes are shown in yellow. (**B**) Red mRFP$^+$, GFP$^-$ LC3 vesicles, corresponding to acidified autolysosomes, were counted and expressed as a percentage of total LC3 vesicles (one-way ANOVA followed by Dunnett's multiple comparison test; $n > 30$ cells; *versus SPG15 unt; +versus ctr). Scale bar = 10 µm. (**C**) SPG15 mutated cells were incubated with the indicated compounds for 24 h, fixed and stained with anti-LAMP1 Ab. The diameter of LAMP1 positive vesicles was determined in two ROI/cell and reported in the graph (one-way ANOVA followed by Dunnett's multiple comparison test; $n = 300$ vesicles; *versus SPG15 unt; +versus ctr). Scale bar = 10 µm.

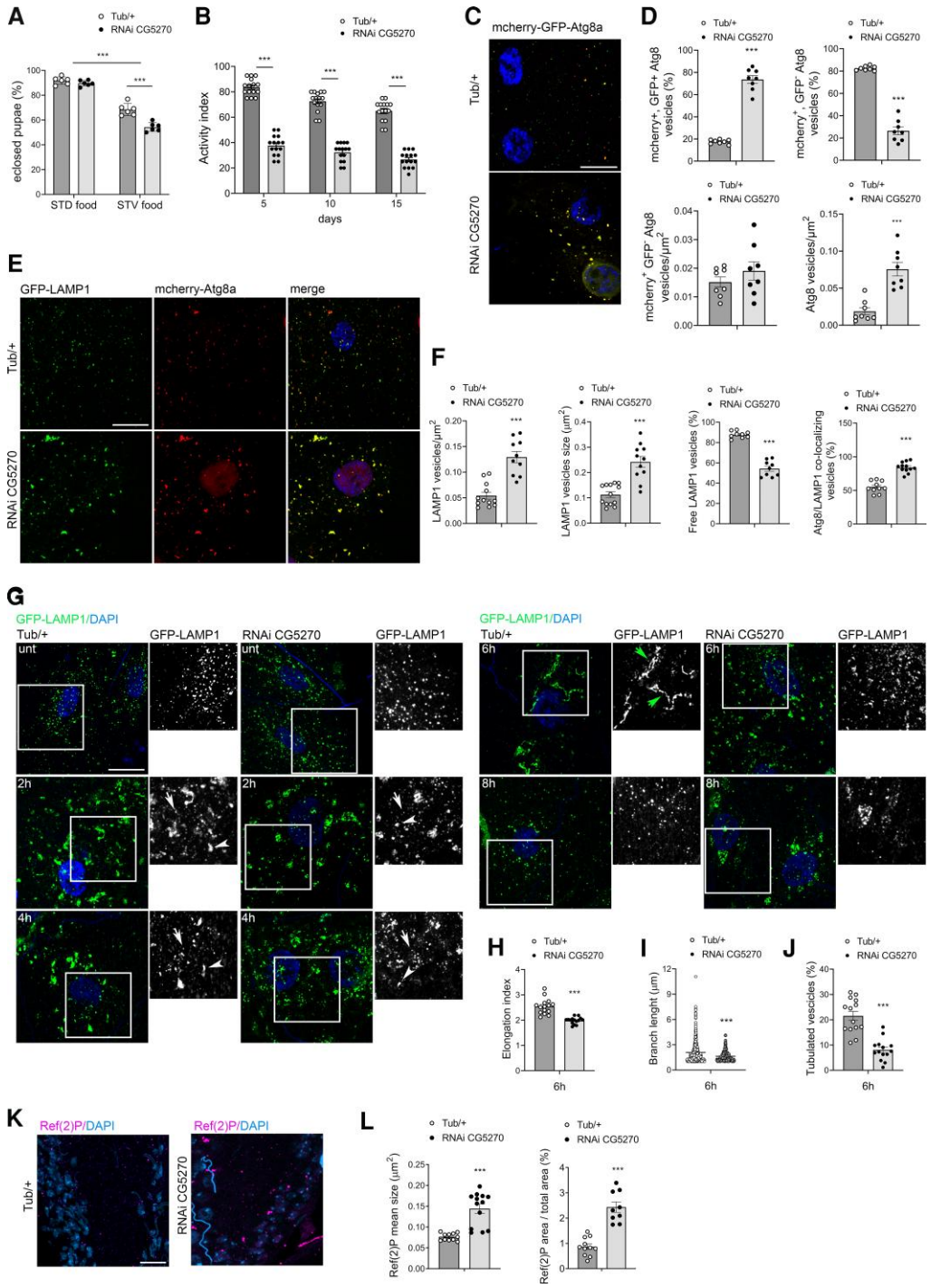

Figure 5 SPG15 *Drosophila* model characterization. (**A**) Eclosion rate of control (Tub/+) and RNAi^{CG5270} lines expressing the Tubulin-Gal4 driver, in standard (STD) and starvation (STV) conditions ($n = 6$ experiments). (**B**) Activity index of negative geotaxis assay of Tub/+ and RNAi^{CG5270} lines measured at 5, 10 and 15 d after eclosion ($n = 15$ experiments). Two-way ANOVA followed by Sidak's multiple comparison test. (**C**) Images show autophagosomes in larval muscles coexpressing RNAi^{CG5270} and mcherry-GFP-Atg8a with the Tubulin driver. Scale bar = 10 µm. (**D**) The graphs show the percentage of autophagosomes (mcherry$^+$, GFP$^+$) and autolysosomes (mcherry$^+$, GFP$^-$ Atg8 vesicles), the number of mcherry$^+$, GFP$^-$ Atg8 vesicles/area and the total number of Atg8 vesicles/area from **C**. Unpaired *t* test; $n = 8$ larvae; *versus Tub/+. (**E**) GFP-LAMP1; mcherry-Atg8a and RNAi^{CG5270} were coexpressed by using the Tubulin driver. Autophagosomes fused with LAMP1 positive vesicles in larval muscles are in yellow. Scale bar = 10 µm. (**F**) The number of LAMP1 positive vesicles/area, the average size of LAMP1 positive organelles, the percentage of free LAMP1 vesicles (not colocalizing with autophagosomes) and of autophagosomes colocalizing with lysosomes/late endosomes (Atg8/LAMP1) from **E** are reported in the graphs. Unpaired *t* test; $n > 9$ larvae; * versus Tub/+. (**G**) Images show LAMP1 positive vesicles in third-instar feeding larvae coexpressing GFP-LAMP1 and RNAi^{CG5270} with the Tubulin driver, starved for 2, 4, 6 and 8 h. The small panels show an higher magnification of the area indicated in the squares. Arrows indicate round and small vesicles, while arrow-heads indicate vesicles that increase in size and decrease in circularity. Green arrows in the magnification of Tub/+ at 6 h indicate tubules extruding from LAMP1 positive vesicles. Area and circularity of LAMP1 positive vesicles and the elongation index of tubulated vesicles from each time points are reported in Supplementary Fig. 9. Scale bar = 10 µm. (**H–J**) Morphometric analysis of LAMP1 positive vesicles from **G**. (**H**) The elongation index of tubulated vesicles ($n = 15$ larvae), (**I**) the branch length of tubules >1 µm ($n > 250$ vesicles) and (**J**) the percentage of vesicles with tubules >1 µm ($n = 14$ larvae) are reported. Unpaired *t* test; * versus Tub/+. (**K**) Third-instar feeding larvae expressing RNAi^{CG5270} with the Tubulin driver were stained with anti Ref(2)P antibody and DAPI. Images show ventral nerve cord of larval brains. Scale bar = 10 µm. (**L**) The mean Ref(2)P aggregates size and the relative Ref(2)P area/ROI area (3400 µm^2) are reported in the graphs (unpaired *t*-test; $n > 9$ larvae; *versus Tub/+).

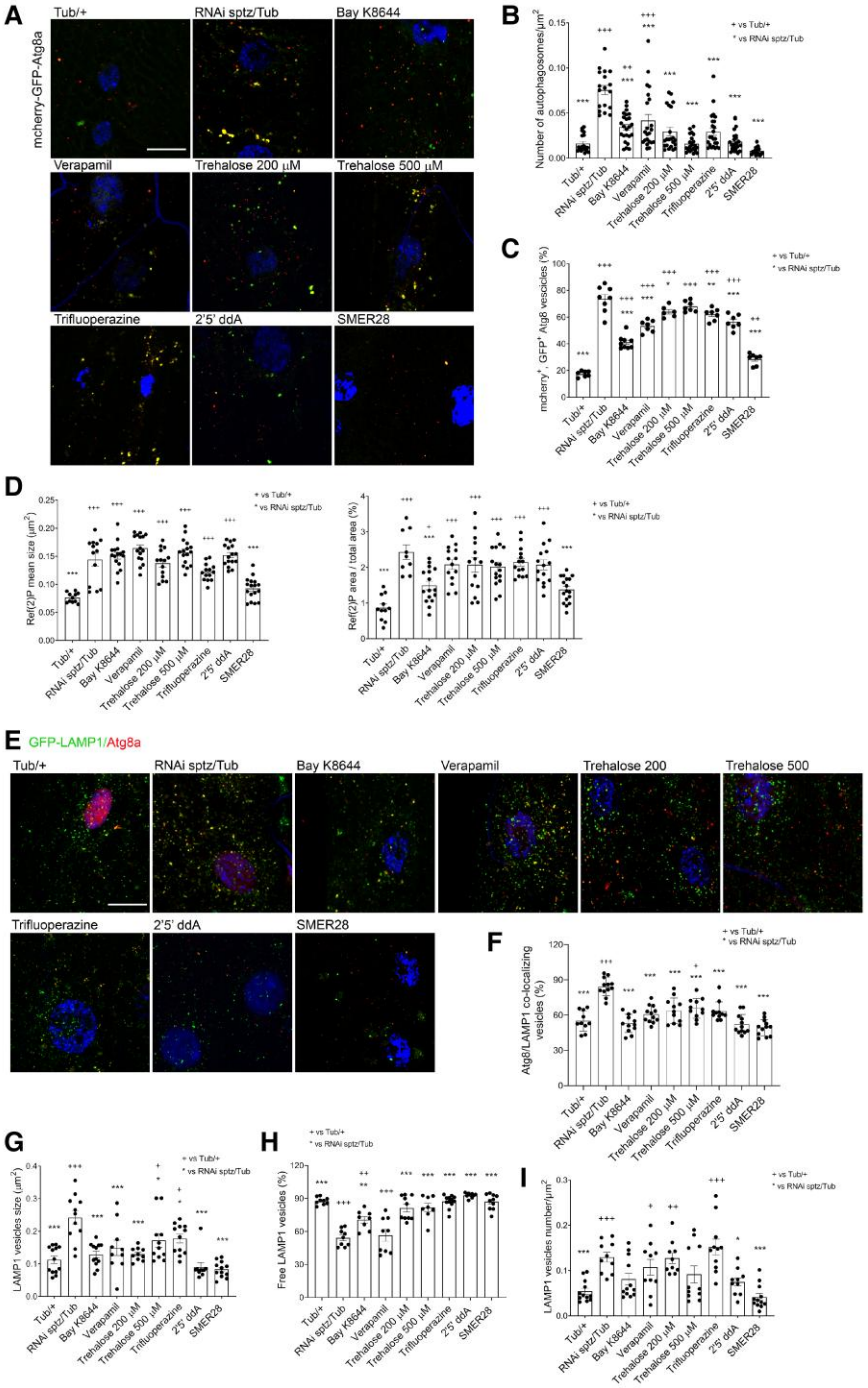

Figure 6 Bay K8644, verapamil, trifluoperazine, 2′,5′-dideoxyadenosine and SMER28 reduce autophagosome accumulation and lysosomal size in a SPG15 *Drosophila* model. (**A**) The mcherry-GFP-Atg8a and the RNAi^{sptz} line were coexpressed by using the Tubulin-Gal4 driver (RNAi sptz/Tub) and chronically treated with 0.4 μM Bay K8644, 1 μM verapamil, 200 and 500 μM trehalose, 30 μM trifluoperazine, 30 μM 2′,5′-dideoxyadenosine (2′5′ ddA) and 20 μM SMER28. Images show autophagosomes in larval muscles. Scale bar = 10 μm. (**B** and **C**) Quantification from **A**. (**B**) The number of autophagosomes/area ($n > 18$ ROI) and (**C**) the percentage of mcherry$^+$, GFP$^+$ Atg8 vesicles (yellow) are reported in the graphs ($n > 8$ larvae). One-way ANOVA followed by Dunnett's multiple comparison test; *versus RNAi sptz/Tub; +versus Tub/+. Comparison data for SMER28 are in Supplementary Tables 7 and 8. (**D**) RNAi sptz/Tub larvae chronically treated with 0.4 μM Bay K8644, 1 μM verapamil, 200 and 500 μM trehalose, 30 μM trifluoperazine, 30 μM 2′,5′-dideoxyadenosine (2′5′ ddA) and 20 μM SMER28, were stained with anti α-Ref(2)P Ab (see Supplementary Fig. 10 for images). The mean Ref(2)P aggregates size and total Ref(2)p area measured in the neurones of the ventral nerve cord are reported (one-way ANOVA followed by Dunnett's multiple comparison test; $n > 10$ larvae; *versus RNAi sptz/Tub; +versus Tub/+). (**E**) The GFP-LAMP1; mcherry-Atg8a and the RNAi^{sptz} lines were coexpressed using the Tubulin-Gal4 driver and chronically treated with 0.4 μM Bay K8644, 1 μM verapamil, 200 and 500 μM trehalose, 30 μM trifluoperazine, 30 μM 2′,5′-dideoxyadenosine (2′5′ ddA) and 20 μM SMER28. Images show LAMP1 positive vesicles (green) and autophagosomes (red) in larval muscles. Scale bar = 10 μm. (**F–I**) Quantification from **E**. (**F**) The percentage of autophagosome colocalizing with LAMP1 positive vesicles (Atg8/LAMP1 positive) ($n > 8$ larvae), (**G**) the LAMP1 vesicles (area) ($n > 8$ larvae), (**H**) the percentage of free LAMP1 vesicles (not colocalizing with autophagosomes) ($n > 8$ larvae) and (**I**) the number of LAMP1 positive vesicles/area ($n > 10$ larvae) are reported in the graphs. One-way ANOVA followed by Dunnett's multiple comparison test; *versus RNAi sptz/Tub; +versus Tub/+.

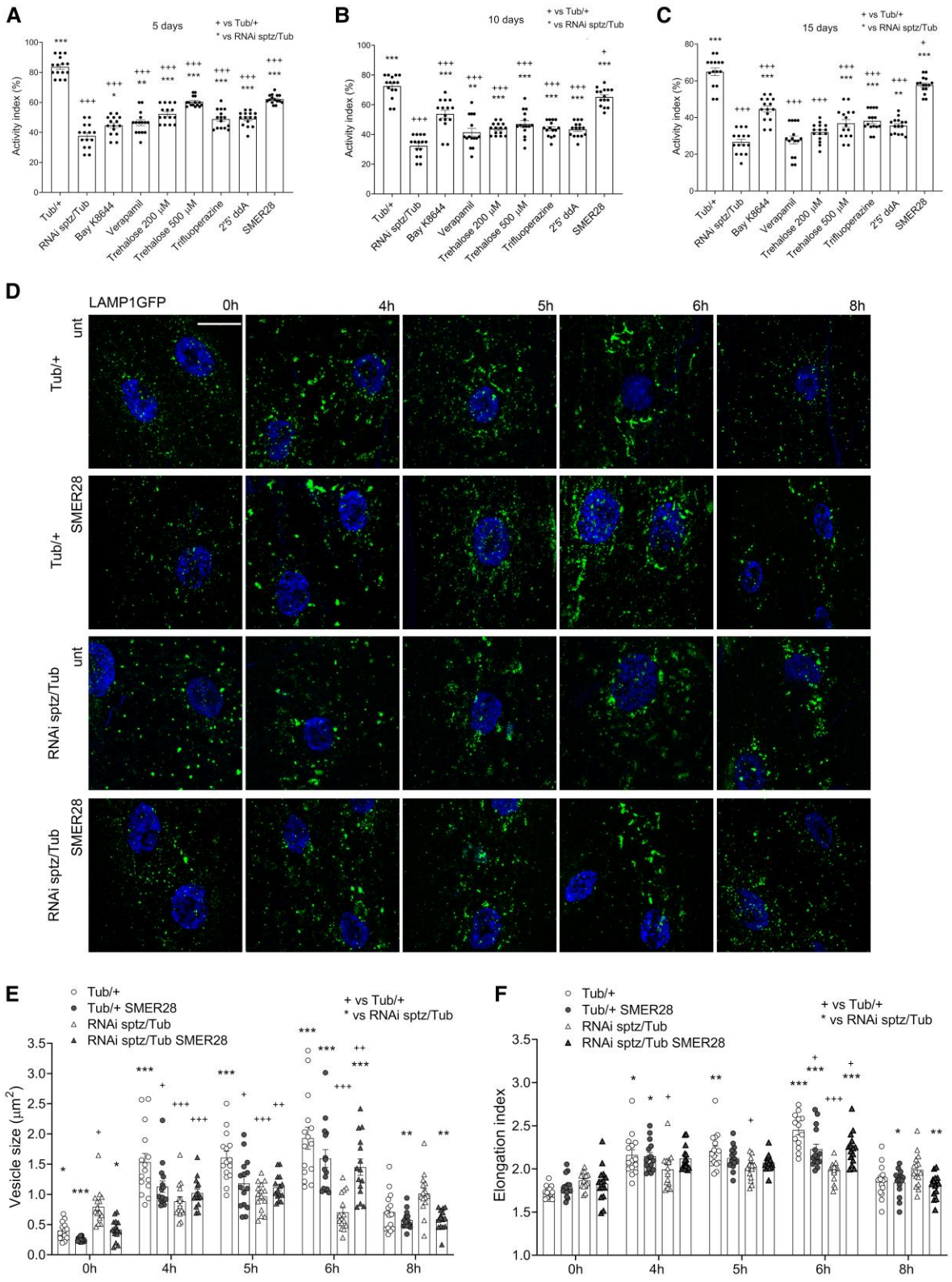

Figure 7 SMER28 rescue locomotion and ALR defects in SPG15 *Drosophila* model. (**A**–**C**) Activity index of negative geotaxis assay of control (Tub/+) and SPG15 *Drosophila* model (RNAi sptz/Tub) measured at 5 (**A**), 10 (**B**) and 15 (**C**) days after eclosion under chronic treatment with 0.4 µM Bay K8644, 1 µM verapamil, 200 and 500 µM trehalose, 30 µM trifluoperazine, 30 µM 2′,5′-dideoxyadenosine (2′5′ ddA) and 20 µM SMER28 (two-way ANOVA followed by Dunnett's multiple comparison test; $n = 15$ experiments; *versus Tub/+). Comparison data for SMER28 are in Supplementary Table 9. (**D**) Third-instar feeding larvae coexpressing LAMP1GFP and RNA^{sptz} with the Tubulin-Gal4 driver line untreated (unt) or chronically treated with 20 µM SMER28 were starved in PBS 20% sucrose for 0, 4, 5, 6 and 8 h. Image show lysosomes. Scale bar = 10 µm. (**E** and **F**) Morphometric analysis of lysosomes of **D**. (**E**) Total vesicle size (area) and (**F**) elongation index of tubulated vesicles are reported in the graphs (two-way ANOVA followed by Dunnett's multiple comparison test; $n = 15$ larvae; *versus Tub/+).

defects, and represents a good SPG15 *Drosophila* model. Therefore, we proposed to name *CG5270 D-Spastizin (D-Sptz)* for the work.

Verapamil, Bay K8644, 2′,5′-dideoxyadenosine and SMER28 rescue lysosomal and autophagy defects in SPG15 *Drosophila* model

We selected verapamil, Bay K8644, 2′,5′-dideoxyadenosine, trehalose, trifluoperazine and SMER28 to rescue autophagy defects in the *Drosophila Sptz* fly model ($RNAi^{sptz}$).

The most effective concentration for each compound with minimal toxic effects was determined (Supplementary Table 5). The effects of the compounds on autophagosome accumulation and degradation in $RNAi^{sptz}$ model were evaluated in larval tissues treated with 0.4 μM Bay K8644, 1 μM verapamil, 200 μM and 500 μM trehalose, 30 μM trifluoperazine, 30 μM 2′,5′-dideoxyadenosine (2′5′ ddA) and 20 μM SMER28 (Fig. 6). All the compounds significantly reduced the number of autophagosomes accumulated in untreated $RNAi^{sptz}$ muscles, although at different threshold levels (Fig. 6A and B), with trehalose, trifluoperazine, 2′,5′-dideoxyadenosine and SMER28 being the most effective (Fig. 6B and Supplementary Table 6). Moreover, all compounds also reduced the number of yellow mcherry+, GFP+ Atg8 vesicles, representing autophagosomes (Fig. 6C), indicating improved lysosomal function and autophagosome degradation. SMER28 was the most efficient (Supplementary Table 7), while only the lowest concentration of trehalose improved degradation. The analysis of Ref(2)P/p62-positive aggregates in $RNAi^{sptz}$ neurones (Fig. 6D and Supplementary Fig. 10) showed that only SMER28 was able to reduce the size of Ref(2)P/p62-positive aggregates, making it effective not only in skeletal muscle, but also in the CNS.

We then analysed the effects of these compounds on lysosomes in the line coexpressing the GFP-LAMP1; mcherry-Atg8a and the $RNAi^{sptz}$ transgenes. All the compounds reduced the accumulation of Atg8a/LAMP1 vesicles (Fig. 6E and F) indicating an increased autolysosome degradation and, except trifluoperazine, also reduced the size of LAMP1 vesicles to values similar to control flies (Fig. 6G). Trehalose, trifluoperazine, 2′,5′-dideoxyadenosine and SMER28 restored the percentage of free LAMP1 vesicles that do not colocalize with autophagosomes and are therefore available for fusion and degradation processes (Fig. 6H). Finally, only 2′,5′-dideoxyadenosine and SMER28 reduced the total number of LAMP1 vesicles (Fig. 6I).

Our data showed also that none of the compounds affected autophagosome number or LAMP1 vesicles size in control muscle or Ref(2)P aggregates in neurones (Supplementary Fig. 11), excluding non-specific effects.

We conclude that only SMER28 was able to restore all the parameters tested *in vivo* in the SPG15 *Drosophila* model.

SMER28 treatment rescues ALR and locomotor defects in SPG15 *Drosophila* model

Chronic treatment of *D-Sptz* loss of function model and quantification of climbing activity at 5, 10 and 15 d (Fig. 7A–C) showed that all the compounds increased flies' locomotor activity indexes at 5 and 10 days. After 15 days, verapamil and 200 μm trehalose did not improve locomotion in the $RNAi^{sptz}$ line, while SMER28 was the most effective compound on this parameter, in line with the results from Ref(2)P aggregates in the nervous system (Fig. 7C and Supplementary Table 8). Therefore, we tested whether SMER28 could also rescue the lysosomal reformation defects in *D-Sptz* fruit fly model. Larvae chronically treated with SMER28 and subjected to starvation (for 4, 5, 6 and 8 h) were processed for immunohistochemistry and lysosomal indexes were quantified. We found that SMER28 was able to partially reconstitute lysosomal homeostasis in larval muscle by stimulating the formation of elongated lysosomes during starvation, and thus suggesting that SMER28 can positively affect ALR *in vivo* (Fig. 7D–F). Therefore, SMER28 could be considered to be a new modulator of lysosomal reformation and a potential therapeutic compound for the SPG15 HSP subtype.

Discussion

SPG15 is an orphan disease: currently, no specific therapy has been developed such that only symptomatic and rehabilitative treatments are available for SPG15 patients. Lysosomal defects and autophagosome accumulation are key players in the pathogenesis of SPG15 and are sensible targets to test novel therapeutic strategies.[16,27,29] Here we report on the identification and further characterization of compounds that are effective *in vivo* in rescuing SPG15 phenotype by targeting lysosomes and autophagy. This was done by screening a library of autophagy-modulating compounds in SPG15-derived cells by which we identified a rose of six compounds that enhanced autophagosome degradation and reduced lysosome/late endosomes enlargement *in vitro* through mTor independent mechanisms.[42,65,74] These six compounds are trehalose, trifluoperazine, SMER28, verapamil, Bay K8644 and 2′,5′-dideoxyadenosine. The *in vivo* administration of each of these compounds in a new SPG15 *Drosophila* model that mimicked the SPG15 phenotype confirmed their positive effects on autophagy and lysosomal deranged processes. The compounds significantly reduced the number of not degraded autolysosomes accumulated in SPG15 *Drosophila* muscles, indicating an improvement in lysosomal function and autophagosome degradation. Beyond the identification of candidate compounds amenable to further pharmacological characterization and therapeutic development, these results indicate that lysosomes are key pharmacological targets to rescue the SPG15 phenotype.

We identified SMER28 as the most effective molecule *in vivo* in restoring autophagosome number, improving autolysosome degradation, increasing the percentage of free available lysosomes and reducing the size of Ref(2)P/p62-positive aggregates in the brain. Moreover, we found that SMER28 rescued ALR defects in SPG15 *Drosophila* muscles and the locomotor deficit observed in this model, supporting its beneficial activity in both neuronal and muscle tissues. Therefore, we propose SMER28 to be a new modulator of lysosomal reformation and a potential therapeutic compound for this HSP subtype.

In more detail, the analysis of the mechanism of these six compounds suggests a possible common action on lysosomes. Trifluoperazine and verapamil both inhibit the TCP2 lysosomal calcium channel, a negative regulator of lysosomal fusion,[75] thereby improving lysosomal functions and fusion.[59,76] Indeed, lysosomal calcium release is involved in lysosome biogenesis and ALR, thus regulating lysosomal calcium channels could improve both processes.[77–80] This also resembles naringenin function, which we found to be effective for SPG31 *Drosophila* model.[41,81] Moreover, trifluoperazine and trehalose both induce TFEB nuclear translocation and the transcription of lysosomal and autophagy regulating genes, promoting lysosome biogenesis.[58,59,74] Concerning Bay K8644 and 2′,5′-dideoxyadenosine, the information is limited and a direct effect on lysosomal functions is not reported. Nevertheless, Bay K8644, as calcium channel modulator, could regulate both plasma membrane and lysosomal channel as reported for the other two

calcium channel modulators, verapamil and trifluoperazine, with similar effects. Moreover, the final effect of calcium channel-regulating compounds on autophagy is not only related to their primary effect on calcium channels, but it could also derive from their chemical propriety or from off-target effects.[82] In line with this, the action of calcium channels regulators on autophagy is not limited to excitable cells, rather, it can also be observed in fibroblasts, hepatocytes and cancer cell lines.[78] Finally, SMER28 induces autophagosome synthesis and improves autophagic flux and autophagosome clearance.[64,65,83,84]

Spastizin, together with Spatacsin, mutated in SPG11, is supposed to participate in the initial step of autophagic lysosomal reformation and both proteins are essential for the process.[27–29] Indeed, Spatacsin and Spastizin may form, or be part of, a lysosome-specific coat that drives fission, either through vesiculation and/or tubulation.[27] Their loss is associated with a failure of ALR with accumulation of autolysosomes and depletion of free lysosomes.[27–29,31] Here we demonstrate that SMER28 promotes ALR *in vivo* and that rescuing ALR is a possible therapeutic strategy for SPG15. Not only do we indicate SMER28 as a potential therapeutic compound for this form of HSP, but also that it can be useful for those associated with ALR and lysosomal defects, such as SPG11. For this HSP subtype, but not for SPG15, two compounds, Miglustat and Tideglusib, have been investigated and their ability to rescue the pathological phenotype was tested. Miglustat reduced lysosomal ganglioside accumulation in cells and zebrafish SPG11 models,[85] but its efficacy for SPG11 patient is uncertain because of its low ability to cross the blood–brain barrier and the increased glycosphingolipid levels reported in the Sandhoff disease mouse model after treatment.[4,86,87] Tideglusib, a GSK3β inhibitor, rescued proliferation and neurodegenerative defects in SPG11 iPSC and organoids.[88,89] Our results, indicating TFEB and its inhibitor GSK3β as therapeutic targets for these forms of HSP, support the possible therapeutic value of Tideglusib. Nevertheless, this needs to be further investigated.

Our analysis also reveals the potential of SMER28, verapamil, Bay K8644, 2′,5′-dideoxyadenosine, trehalose and trifluoperazine for other HSP subtypes associated with autophagy/lysosomal defects, such as SPG11, SPG48, SPG49 and SPG78, and for neurodegenerative diseases associated with lysosomal dysfunctions, such as lysosomal storage disorders, amyotrophic later sclerosis and ataxia.[26] All six compounds have been widely tested for their therapeutic potentiality in several neurodegenerative disease models, albeit at different extents.[42,90–97] Notably, SMER28 is reported to: (i) prevent beta-amyloid aggregate formation and reduce accumulation in cellular models of Alzheimer's disease[74,96]; (ii) enhance the clearance of mutant huntingtin in Huntington's disease cells and *Drosophila* models[64]; and (iii) attenuate dopaminergic neuronal degeneration and improving motor behaviour in a Parkinson's disease rat model.[98] In addition, verapamil and trifluoperazine are clinically used compounds to treat cardiovascular disease and psychosis, respectively, and repositioning tests are ongoing for different neurodegenerative disorders. Two clinical trials for the use of trehalose in SPG11 and neuronal ceroid lipofuscinoses patients are active (NCT04912609 and NCT04808297; ClinicalTrials.gov). No clinical trials instead are registered for SMER28, Bay K8644 and 2′,5′-dideoxyadenosine, which therefore need to be further investigated. The efficacy of SMER28 at post-symptomatic stages in the SPG15 fly model encourages a future translation in clinics.

In conclusion, the identification of a number of molecules as potential candidates for a pharmacological intervention in HSP is of great relevance in the HSP field because of the lack of gene-specific pharmacological therapy.[8,9] Indeed, rehabilitation along with symptomatic treatments are so far the only treatments available for this disease. However, considering the various degrees of diseases severity observed in SPG15 and in other HSP subtypes with similar autophagy/lysosomal defects, the combined approach of a rehabilitative intervention and a pharmacological treatment is likely to represent the most effective disease therapy. Based on this, a number of molecules rather than a single one may be necessary to reach this goal. In line with that, the findings here reported all represent valuable data to select the best candidate/s to start with.

Funding

This work was supported by funds from Ministero della Salute (Ricerca Corrente grant no. RC 2021-2022 and RF-2019-12370112 to M.T.B.), from Fondazione Regionale per la Ricerca Biomedica (FRRB) (grant no. Care4Neurorare to M.T.B.), from the University of Padova (PRIDJ 18_01 to G.O.) and Fondazione Cariparo (Young Investigator Grant on Pediatric Research to G.O.). G.G. is a recipient of a fellowship from the University of Padova.

Competing interests

The authors report no competing interests

Supplementary material

Supplementary material is available at *Brain* online

References

1. Fink JK. Hereditary spastic paraplegia. *Curr Neurol Neurosci Rep*. 2006;6(1):65–76.
2. Depienne C, Fedirko E, Faucheux JM, *et al*. A de novo SPAST mutation leading to somatic mosaicism is associated with a later age at onset in HSP. *Neurogenetics*. 2007;8(3):231–3.
3. Blackstone C. Converging cellular themes for the hereditary spastic paraplegias. *Curr Opin Neurobiol*. 2018;51:139–46.
4. Darios F, Mochel F, Stevanin G. Lipids in the physiopathology of hereditary spastic paraplegias. *Front Neurosci*. 2020;14:74.
5. Elsayed LEO, Eltazi IZ, Ahmed AE, Stevanin G. Insights into clinical, genetic, and pathological aspects of hereditary spastic paraplegias: A comprehensive overview. *Front Mol Biosci*. 2021;8:690899.
6. Tadepalle N, Rugarli EI. Lipid droplets in the pathogenesis of hereditary spastic paraplegia. *Front Mol Biosci*. 2021;8:673977.
7. Toupenet Marchesi L, Leblanc M, Stevanin G. Current knowledge of endolysosomal and autophagy defects in hereditary spastic paraplegia. *Cells*. 2021;10(7):1678.
8. Bellofatto M, De Michele G, Iovino A, Filla A, Santorelli FM. Management of hereditary spastic paraplegia: A systematic review of the literature. *Front Neurol*. 2019;10:3.
9. Lallemant-Dudek P, Darios F, Durr A. Recent advances in understanding hereditary spastic paraplegias and emerging therapies. *Fac Rev*. 2021;10:27.
10. Hanein S, Martin E, Boukhris A, *et al*. Identification of the SPG15 gene, encoding spastizin, as a frequent cause of complicated autosomal-recessive spastic paraplegia, including Kjellin syndrome. *Am J Hum Genet*. 2008;82(4):992–1002.
11. Schüle R, Schlipf N, Synofzik M, *et al*. Frequency and phenotype of SPG11 and SPG15 in complicated hereditary spastic paraplegia. *J Neurol Neurosurg Psychiatry*. 2009;80(12):1402–4.

12. Hirst J, Borner GH, Edgar J, *et al*. Interaction between AP-5 and the hereditary spastic paraplegia proteins SPG11 and SPG15. *Mol Biol Cell*. 2013;24(16):2558–69.
13. Stevanin G, Azzedine H, Denora P, *et al*. Mutations in SPG11 are frequent in autosomal recessive spastic paraplegia with thin corpus callosum, cognitive decline and lower motor neuron degeneration. *Brain*. 2008;131(Pt3):772–84.
14. Pensato V, Castellotti B, Gellera C, *et al*. Overlapping phenotypes in complex spastic paraplegias SPG11, SPG15, SPG35 and SPG48. *Brain*. 2014;137(Pt 7):1907–20.
15. Słabicki M, Theis M, Krastev DB, *et al*. A genome-scale DNA repair RNAi screen identifies SPG48 as a novel gene associated with hereditary spastic paraplegia. *PLoS Biol*. 2010;8(6):e1000408.
16. Vantaggiato C, Crimella C, Airoldi G, *et al*. Defective autophagy in spastizin mutated patients with hereditary spastic paraparesis type 15. *Brain*. 2013;136(Pt10):3119–39.
17. Vantaggiato C, Clementi E, Bassi MT. ZFYVE26/SPASTIZIN: A close link between complicated hereditary spastic paraparesis and autophagy. *Autophagy*. 2014;10(2):374–5.
18. Vantaggiato C, Panzeri E, Castelli M, *et al*. ZFYVE26/SPASTIZIN and SPG11/SPATACSIN mutations in hereditary spastic paraplegia types AR-SPG15 and AR-SPG11 have different effects on autophagy and endocytosis. *Autophagy*. 2019;15(1):34–57.
19. Yu L, McPhee CK, Zheng L, *et al*. Termination of autophagy and reformation of lysosomes regulated by mTOR. *Nature*. 2010;465-(7300):942–6.
20. Chen Y, Yu L. Autophagic lysosome reformation. *Exp Cell Res*. 2013;319(2):142–6.
21. Wong ASL, Cheung ZH, Ip NY. Molecular Machinery of macroautophagy and its deregulation in diseases. *Biochim Biophys Acta*. 2011;1812(11):1490–7.
22. Lumkwana D, du Toit A, Kinnear C, Loos B. Autophagic flux control in neurodegeneration: Progress and precision targeting—Where do we stand? *Prog Neurobiol*. 2017;153:64–85.
23. Sarkar S. Regulation of autophagy by mTOR-dependent and mTOR-independent pathways: Autophagy dysfunction in neurodegenerative diseases and therapeutic application of autophagy enhancers. *Biochem Soc Trans*. 2013;41(5):1103–30.
24. Menzies FM, Fleming A, Rubinsztein DC. Compromised autophagy and neurodegenerative diseases. *Nat Rev Neurosci*. 2015;16(6):345–57.
25. Frake RA, Ricketts T, Menzies FM, Rubinsztein DC. Autophagy and neurodegeneration. *J Clin Invest*. 2015;125(1):65–74.
26. Darios F, Stevanin G. Impairment of lysosome function and autophagy in rare neurodegenerative diseases. *J Mol Biol*. 2020;432(8):2714–34.
27. Chang J, Lee S, Blackstone C. Spastic paraplegia proteins spastizin and spatacsin mediate autophagic lysosome reformation. *J Clin Invest*. 2014;124(12):5249–62.
28. Varga RE, Khundadze M, Damme M, *et al*. *In vivo* evidence for lysosome depletion and impaired autophagic clearance in hereditary spastic paraplegia type SPG11. *PLoS Genet*. 2015;11(8):e1005454.
29. Khundadze M, Ribaudo F, Hussain A, *et al*. Mouse models for hereditary spastic paraplegia uncover a role of PI4K2A in autophagic lysosome reformation. *Autophagy*. 2021;17(11):3690–706.
30. Renvoisé B, Chang J, Singh R, *et al*. Lysosomal abnormalities in hereditary spastic paraplegia types SPG15 and SPG11. *Ann Clin Transl Neurol*. 2014;1(6):379–89.
31. Marrone L, Marchi PM, Webster CP, *et al*. SPG15 protein deficits are at the crossroads between lysosomal abnormalities, altered lipid metabolism and synaptic dysfunction. *Hum Mol Genet*. 2022;31:2693–710.
32. Khundadze M, Kollmann K, Koch N, *et al*. A hereditary spastic paraplegia mouse model supports a role of ZFYVE26/SPASTIZIN for the endolysosomal system. *PLoS Genet*. 2013;9-(12):e1003988.
33. Kimura S, Noda T, Yoshimori T. Dissection of the autophagosome maturation process by a novel reporter protein, tandem fluorescent-tagged LC3. *Autophagy*. 2007;3(5):452–60.
34. Mushtaq Z, Choudhury SD, Gangwar SK, Orso G, Kumar V. Human senataxin modulates structural plasticity of the neuromuscular junction in *Drosophila* through a neuronally conserved TGFβ signalling pathway. *Neurodegener Dis*. 2016;16(5-6):324–36.
35. Dagda RK, Cherra SJ 3rd, Kulich SM, Tandon A, Park D, Chu CT. Loss of PINK1 function promotes mitophagy through effects on oxidative stress and mitochondrial fission. *J Biol Chem*. 2009;284-(20):13843–55.
36. Wiemerslage L, Lee D. Quantification of mitochondrial morphology in neurites of dopaminergic neurones using multiple parameters. *J. Neurosci. Methods*. 2016;262:56–65.
37. Vantaggiato C, Castelli M, Giovarelli M, *et al*. The fine tuning of Drp1-dependent mitochondrial remodeling and autophagy controls neuronal differentiation. *Front Cell Neurosci*. 2019;13:120.
38. Valente AJ, Maddalena LA, Robb EL, Moradi F, Stuart JA. A simple ImageJ macro tool for analyzing mitochondrial network morphology in mammalian cell culture. *Acta Histochem*. 2017;119(3):315–26.
39. Wu S, Tan KJ, Govindarajan LN, *et al*. Fully automated leg tracking of *Drosophila* neurodegeneration models reveals distinct conserved movement signatures. *PLoS Biol*. 2019;17(6):e3000346.
40. Fantin M, Garelli F, Napoli B, *et al*. Flavonoids regulate lipid droplets biogenesis in *Drosophila melanogaster*. *Natural Product Communications*. 2019;14(5):1934578X1985243.
41. Napoli B, Gumeni S, Forgiarini A, *et al*. Naringenin ameliorates *Drosophila* ReepA hereditary spastic paraplegia-linked phenotypes. *Front Neurosci*. 2019;13:1202.
42. Williams A, Sarkar S, Cuddon P, *et al*. Novel targets for Huntington's disease in an mTOR-independent autophagy pathway. *Nat Chem Biol*. 2008;4(5):295–305.
43. Zhou M, Wang R. Small-molecule regulators of autophagy and their potential therapeutic applications. *ChemMedChem*. 2013;8(5):694–707.
44. Vakifahmetoglu-Norberg H, Xia HG, Yuan J. Pharmacologic agents targeting autophagy. *J Clin Invest*. 2015;125(1):5–13.
45. Cho YS, Kwon HJ. Control of autophagy with small molecules. *Arch Pharm Res*. 2010;33(12):1881–9.
46. Bergson P, Lipkind G, Lee SP, Duban ME, Hanck DA. Verapamil block of T-type calcium channels. *Mol Pharmacol*. 2011;79(3):411–9.
47. Gould RJ, Murphy KM, Reynolds IJ, Snyder SH. Antischizophrenic drugs of the diphenylbutylpiperidine type act as calcium channel antagonists. *Proc Natl Acad Sci USA*. 1983;80(16):5122–5.
48. Xia H-G, Zhang L, Chen G, *et al*. Control of basal autophagy by calpain1 mediated cleavage of ATG5. *Autophagy*. 2010;6:61–6.
49. Greenberg DA, Cooper EC, Carpenter CL. Calcium channel 'agonist' BAY K 8644 inhibits calcium antagonist binding to brain and PC12 cell membranes. *Brain Res*. 1984;305(2):365–8.
50. Itakura E, Mizushima N. p62 Targeting to the autophagosome formation site requires self-oligomerization but not LC3 binding. *J Cell Biol*. 2011;192(1):17–27.
51. Kumar AV, Mills J, Lapierre LR. Selective autophagy receptor p62/SQSTM1, a pivotal player in stress and aging. *Front Cell Dev Biol*. 2022;10:793328.
52. Renna M, Jimenez-Sanchez M, Sarkar S, Rubinsztein DC. Chemical inducers of autophagy that enhance the clearance

of mutant proteins in neurodegenerative diseases. *J Biol Chem*. 2010;285(15):11061–7.
53. Sarkar S, Floto RA, Berger Z, *et al*. Lithium induces autophagy by inhibiting inositol monophosphatase. *J Cell Biol*. 2005;170(7): 1101–1.
54. Williams RS, Cheng L, Mudge AW, Harwood AJ. A common mechanism of action for three mood-stabilizing drugs. *Nature*. 2002;417(6886):292–5.
55. Viana R, Aguado C, Esteban I, *et al*. Role of AMP-activated protein kinase in autophagy and proteasome function. *Biochem Biophys Res Commun*. 2008;369(3):964–8.
56. Yan J, Yan JY, Wang YX, *et al*. Spermidine-enhanced autophagic flux improves cardiac dysfunction following myocardial infarction by targeting the AMPK/mTOR signalling pathway. *Br J Pharmacol*. 2019;176(17):3126–42.
57. Yang Y, Chen S, Zhang Y, *et al*. Induction of autophagy by spermidine is neuroprotective via inhibition of caspase 3-mediated Beclin 1 cleavage. *Cell Death Dis*. 2017;8(4):e2738.
58. Rusmini P, Cortese K, Crippa V, *et al*. Trehalose induces autophagy via lysosomal-mediated TFEB activation in models of motoneuron degeneration. *Autophagy*. 2019;15(4):631–51.
59. Zhang Y, Nguyen DT, Olzomer EM, *et al*. Rescue of pink1 deficiency by stress-dependent activation of autophagy. *Cell Chem Biol*. 2017;24(4):471–80.e4.
60. Settembre C, Di Malta C, Polito VA, *et al*. TFEB links autophagy to lysosomal biogenesis. *Science*. 2011;332(6036):1429–33.
61. Ren F, Zhang L, Zhang X, *et al*. Inhibition of glycogen synthase kinase 3β promotes autophagy to protect mice from acute liver failure mediated by peroxisome proliferator-activated receptor α. *Cell Death Dis*. 2016;7(3):e2151.
62. Parr C, Carzaniga R, Gentleman SM, Van Leuven F, Walter J, Sastre M. Glycogen synthase kinase 3 inhibition promotes lysosomal biogenesis and autophagic degradation of the amyloid-β precursor protein. *Mol Cell Biol*. 2012;32(21):4410–8.
63. Li Y, Xu M, Ding X, *et al*. Protein kinase C controls lysosome biogenesis independently of mTORC1. *Nat Cell Biol*. 2016;18(10): 1065–77.
64. Sarkar S, Perlstein EO, Imarisio S, *et al*. Small molecules enhance autophagy and reduce toxicity in Huntington's disease models. *Nat Chem Biol*. 2007;3(6):331–8.
65. Koukourakis MI, Giatromanolaki A, Fylaktakidou K, *et al*. SMER28 is a mTOR-independent small molecule enhancer of autophagy that protects mouse bone marrow and liver against radiotherapy. *Invest New Drugs*. 2018;36(5):773–81.
66. Cheng XT, Xie YX, Zhou B, Huang N, Farfel-Becker T, Sheng ZH. Characterization of LAMP1-labeled nondegradative lysosomal and endocytic compartments in neurons. *J Cell Biol*. 2018; 217(9):3127–39.
67. Gaudet P, Livstone MS, Lewis SE, Thomas PD. Phylogenetic-based propagation of functional annotations within the Gene Ontology consortium. *Brief Bioinform*. 2011;12(5):449–62.
68. Orso G, Martinuzzi A, Rossetto MG, Sartori E, Feany M, Daga A. Disease-related phenotypes in a *Drosophila* model of hereditary spastic paraplegia are ameliorated by treatment with vinblastine. *J Clin Invest*. 2005;115(11):3026–34.
69. Julien C, Lissouba A, Madabattula S, *et al*. Conserved pharmacological rescue of hereditary spastic paraplegia-related phenotypes across model organisms. *Hum Mol Genet*. 2016;25(6): 1088–99.
70. Gan-Or Z, Bouslam N, Birouk N, *et al*. Mutations in CAPN1 cause autosomal-recessive hereditary spastic paraplegia. *Am J Hum Genet*. 2016;98(5):1038–46.
71. Murakawa T, Kiger AA, Sakamaki Y, Fukuda M, Fujita N. An autophagy-dependent tubular lysosomal network synchronizes degradative activity required for muscle remodeling. *J Cell Sci*. 2020;133(21):jcs248336.
72. De Filippis C, Napoli B, Rigon L, *et al*. *Drosophila* D-idua reduction mimics mucopolysaccharidosis type I disease-related phenotypes. *Cells*. 2021;11(1):129.
73. McGrath MJ, Eramo MJ, Gurung R, *et al*. Defective lysosome reformation during autophagy causes skeletal muscle disease. *J Clin Invest*. 2021;131(1):e135124.
74. Sarkar S, Davies JE, Huang Z, Tunnacliffe A, Rubinsztein DC. Trehalose, a novel mTOR-independent autophagy enhancer, accelerates the clearance of mutant huntingtin and alpha-synuclein. *J Biol Chem*. 2007;282(8):5641–52.
75. Zhang R, Kang R, Klionsky DJ, Tang D. Ion channels and transporters in autophagy. *Autophagy*. 2022 18:4–23.
76. Jin X, Zhang Y, Alharbi A, Hanbashi A, Alhoshani A, Parrington J. Targeting two-pore channels: current progress and future challenges. *Trends Pharmacol Sci*. 2020;41(8):582–94.
77. Medina DL, Di Paola S, Peluso I, *et al*. Lysosomal calcium signalling regulates autophagy through calcineurin and TFEB. *Nat Cell Biol*. 2015;17(3):288–99.
78. Cao Q, Yang Y, Zhong XZ, Dong XP. The lysosomal Ca2+ release channel TRPML1 regulates lysosome size by activating calmodulin. *J Biol Chem*. 2017;292(20):8424–35.
79. Ballabio A, Bonifacino JS. Lysosomes as dynamic regulators of cell and organismal homeostasis. *Nat Rev Mol Cell Biol*. 2020;21: 101–18.
80. Rosato AS, Tang R, Grimm C. Two-pore and TRPML cation channels: regulators of phagocytosis, autophagy and lysosomal exocytosis. *Pharmacol Ther*. 2021;220:107713.
81. Gumeni S, Vantaggiato C, Montopoli M, Orso G. Hereditary spastic paraplegia and future therapeutic directions: beneficial effects of small compounds acting on cellular stress. *Front Neurosci*. 2021;15:660714.
82. Kondratskyi A, Kondratska K, Skryma R, Klionsky DJ, Prevarskaya N. Ion channels in the regulation of autophagy. *Autophagy*. 2018;14(1):3–21.
83. Tian Y, Bustos V, Flajolet M, Greengard P. A small-molecule enhancer of autophagy decreases levels of Abeta and APP-CTF via Atg5-dependent autophagy pathway. *FASEB J*. 2011;25(6): 1934–42.
84. Kalamida D, Karagounis IV, Giatromanolaki A, Koukourakis MI. Important role of autophagy in endothelial cell response to ionizing radiation. *PLoS ONE*. 2014;9(7):e102408.
85. Boutry M, Branchu J, Lustremant C, *et al*. Inhibition of lysosome membrane recycling causes accumulation of gangliosides that contribute to neurodegeneration. *Cell Rep*. 2018;23(13):3813–26.
86. Schiffmann R, Fitzgibbon EJ, Harris C, *et al*. Randomized, controlled trial of miglustat in Gaucher's disease type 3. *Ann Neurol*. 2008;64(5):514–22.
87. Ashe KM, Bangari D, Li L, *et al*. Iminosugar-based inhibitors of glucosylceramide synthase increase brain glycosphingolipids and survival in a mouse model of Sandhoff disease. *PLoS ONE*. 2011;6(6):e21758.
88. Mishra HK, Prots I, Havlicek S, *et al*. GSK3ß-dependent dysregulation of neurodevelopment in SPG11-patient induced pluripotent stem cell model. *Ann Neurol*. 2016;79(5):826–40.
89. Pérez-Brangulí F, Buchsbaum IY, Pozner T, *et al*. Human SPG11 cerebral organoids reveal cortical neurogenesis impairment. *Hum Mol Genet*. 2019;28(6):961–71.
90. Zhang X, Chen S, Lu K, *et al*. Verapamil ameliorates motor neuron degeneration and improves lifespan in the SOD1^{G93A}Mouse model of ALS by enhancing autophagic flux. *Aging Dis*. 2019; 10(6):1159–73.

91. Popović N, Morales-Delgado N, Vidal Mena D, *et al*. Verapamil and Alzheimer's disease: Past, present, and future. *Front Pharmacol*. 2020;11:562.
92. Höllerhage M, Goebel JN, de Andrade A, *et al*. Trifluoperazine rescues human dopaminergic cells from wild-type α-synuclein-induced toxicity. *Neurobiol Aging*. 2014;35(7):1700–11.
93. Castillo K, Nassif M, Valenzuela V, *et al*. Trehalose delays the progression of amyotrophic lateral sclerosis by enhancing autophagy in motoneurones. *Autophagy*. 2013;9(9):1308–20.
94. Du J, Liang Y, Xu F, Sun B, Wang Z. Trehalose rescues Alzheimer's disease phenotypes in APP/PS1 transgenic mice. *J Pharm Pharmacol*. 2013;65(12):1753–6.
95. Hu HH, Li SJ, Wang P, *et al*. An L-type calcium channel agonist, bay K8644, extends the window of intervention against ischemic neuronal injury. *Mol Neurobiol*. 2013;47(1):280–9.
96. Armstrong GA, Drapeau P. Calcium channel agonists protect against neuromuscular dysfunction in a genetic model of TDP-43 mutation in ALS. *J Neurosci*. 2013;33(4):1741–52.
97. Pierzynowska K, Gaffke L, Cyske Z, *et al*. Autophagy stimulation as a promising approach in treatment of neurodegenerative diseases. *Metab Brain Dis*. 2018;33(4):989–1008.
98. Darabi S, Noori-Zadeh A, Rajaei F, *et al*. SMER28 attenuates dopaminergic toxicity mediated by 6-hydroxydopamine in the rats via modulating oxidative burdens and autophagy-related parameters. *Neurochem Res*. 2018;43(12):2313–23.